A GLOBAL POSITIONING SYSTEM ON THE LUNAR SPHERE UTILIZING CUBESATS

A Thesis

Presented to the

Faculty of

California State University,

San Bernardino

In Partial Fulfillment

of the Requirements for the Degree

Master of Science

in

Computer Science

---

by

Armani Giann Batista

June 2012

A GLOBAL POSITIONING SYSTEM ON THE LUNAR SPHERE UTILIZING CUBESATS

A Thesis

Presented to the

Faculty of

California State University,

San Bernardino

---

by

Armani Giann Batista

June 2012

Approved by:

Dr. Keith Evan Schubert, Advisor, School of Computer Science and Engineering	Date
Dr. Ernesto Gomez	
Dr. Haiyan Qiao	

ABSTRACT

The Global Positioning System (GPS) is quickly becoming a ubiquitous navigation system being used in cars, cell phones, airplanes, and many other areas of our lives. Upon astronauts returning to the moon, navigation will be just as crucial for exploration and safety. The research conducted for this thesis shows that a Lunar GPS could be developed using CubeSats and chip-scale atomic clocks (CSAC). The rationale for utilizing the CubeSat platform is to reduce the costs that are currently associated with GPS satellites under a flight proven platform. The satellite constellation considers a Rider inclined circular orbit of two planes and eight satellites per plane at an altitude of 3.34×10^4 km. Also, the estimated time between clock updates for this system is 5.56 $\frac{min}{m}$. Furthermore, a high-level design of such a system is presented integrating the analysis of multiple points of research and various numerical algorithms pertaining to GPS. Included are error analyses from the noise caused by the lunar ionosphere, clock drift from the CSAC, QR factorization of the least squares problem for user position, velocity, and time determination, and Kalman filtering for optimization. Future directions may include the design and development for the architecture of this proposed Lunar CubeSat GPS.

ACKNOWLEDGEMENTS

I would like to extend my gratitude to my committee members: Dr. Ernesto Gomez and Dr. Haiyain Qiao, for their assistance and support not only with this thesis, but throughout my undergraduate and graduate education. Special thanks to Dr. Voigt for her support with my entrance into the graduate program. I also want to thank my advisor Dr. Keith Schubert who has been an incredible mentor over the past five years. Thank you to my supporting family and friends. Thank you to my fiance Rosa for helping, believing, and pushing me to complete this thesis. Most of all, my deepest thank you to the Alpha and Omega, I AM, the God of Abraham, Isaac, and Jacob, my Father, my Lord and Savior Jesus Christ, and the Holy Spirit. This thesis and I exist by His grace.

DEDICATION

In Memory of Ito: (December 27, 1942 - January 2, 2010)

TABLE OF CONTENTS

LIST OF FIGURES

1. INTRODUCTION

1.1 Thesis Overview

1.1.1 Purpose

The purpose of this thesis was to research: the viability and feasibility of a new Lunar GPS that would utilize the CubeSat platform, newly emerging technology, and the consideration of satellites without the large, currently employed, chemical atomic clocks. This also achieves the underlying goal of decreasing the currently associated costs of GPS.

1.1.2 Motivation

This research is motivated by future manned and unmanned missions to the moon and other terrestrial, heavenly bodies such as Mars, moons of other solar system planets, and large asteroids. Since navigation on these bodies will be critical for the success of the missions and moreover the safety of the astronauts, a new and cost effective GPS is needed.

1.2 Document Organization

The major content of this thesis is organized as follows. First, the following sections will discuss the influential references and contributions of this research. Chapter two

will provide a brief introduction of orbital mechanics and GPS in general referencing an Earth based system to bring the reader up to speed on these topics. Next, chapter three will discuss the satellite constellation design. In chapter four the CubeSats themselves along with the new atomic clock will be described. Chapter five will expand on the major causes of errors that affect GPS, and present a numerical algorithm for estimating pseudoranges, position, velocity, and time (PVT). Subsequently, chapter six will describe an optimization algorithm. In chapter seven, everything is summarized, the conclusion is made, and the possibilities for future research are presented. Lastly, it should be noted that all test programs to support this research were written in Scilab, and are can be found on the accompanying CD.

1.3 Literature Review

GPS has been available now for several years, and its technology and theories are fairly well understood. Since an introduction to it will be provided shortly, the paragraph below mentions the major references that helped contribute to the research conducted on designing a lunar GPS.

The CubeSat platform developed by California Polytechnic State University San Luis Obispo and Stanford University has created a robust, low-cost standard for picosatellites [16, 17]. This allows for many groups, entities, and companies to conduct satellite research which was once before out of their grasp. Due to the stringent volume and max payload weight of the CubeSat, a conventional Atomic Frequency Standard (AFS) will not fit. For instance, the size and weight of the AFS used on-board the IIR block NAVSTAR GPS satellites is about $227m^3$ ($3700cm^3$) and

12lbs (5.4kg), however, the total volume of the CubeSat is only $1000cm^3$ with a max payload weight of 1kg [16, 17, 39]. Therefore, a new type of AFS was needed. In this thesis it is proposed to use the newly emerging chip-scale atomic clock (CSAC) [18]. New improvements and research has been conducted on using coherent population trapping (CPT) for AFSs with some of the major contributors being S. Knappe, J. Kitching, and L. Hollberb among others [18, 19]. CPT and CSAC are discussed further in chapter four.

With the satellite constellation design, the equation derived by L. Rider for determining optimal coverage of satellites around the Earth was used as a basis for lunar coverage [15, 46]. The implications of his work provide an optimal method for calculating the fewest required satellites to ensure global coverage [1]. More on this topic will be presented in chapter three where the Rider constellation is shown for inclined circular orbits. During the course of this research it was also found that NASA had discovered the moon indeed has an ionosphere [14]. This discovery dates back as far as the Apollo missions, but had never been qualified until recently by T.J. Stubbs of NASA [14, 20, 21]. It is postulated that the explanation for the lunar ionosphere is from ionized dust particles in the lunar atmosphere [14, 20, 21]. This is important because of the adverse affects on signals sent from orbiting space vehicles down to the lunar surface, producing errors in PVT determination thereby lowering its accuracy [1]. Assuming the ionosphere is the result of ionized dust particles, it should increase as human exploration expands considering our presence would cause more dust to be dispersed into the atmosphere. Two researchers from the University of Illinois (Rysanek and Hartmann) designed an innovative vacuum arc thruster for

their satellite the Illinois Observing Nanosatellite (ION) [25]. The implications of their research created a thruster which can propel the satellite without the use of pyrotechnics which are not permitted within the CubeSat specification [25].

In 2008, a lunar GPS system had begun research and development by Ron Li in partnership with NASA [41]. This system is a differential GPSI which works by a sensor and data network [42]. Their system only uses pre-orbiting or soon to be launched satellites, and does not have a dedicated satellite system. This system has already begun field testing in Washington and Arizona [44]. Subsequently, the research in this thesis can be used in cooperation not competition with such a system to improve PVT accuracy and position. Finally, there was a thesis conducted by V. Daita where he implemented a GPS receiver using VHDL [45]. His work shows that a system on a chip (SOC) is a viable solution for the implementation of a GPS receiver, and that these ideas do not have to be implemented as a series of discrete devices [45].

1.4 Contributions

From the research conducted for this thesis, it will be shown that atomic clocks exist which are small enough to be implemented within the constraints of the CubeSat platform. Next, it will be discussed that the CubeSat platform is theoretically a viable option for implementing a Lunar GPS. With the proposed high level design for such a system, a satellite constellation design is presented using Rider inclined circular orbits. Subsequently this research was accepted into the WorldComp'12 conference [46]. Additionally, the formerly mentioned thruster system is suggested as a possibility for correcting the satellite's trajectory. Furthermore, a review of

the aforementioned lunar ionosphere is related to the GPS. Then, the numerical analysis employing a least squares solution utilizing QR factorization will be shown to calculate pseudoranges, position, velocity, and time. Subsequently, the Kalman filter is applied to the least squares solution to compute an optimal estimation of these values. It is worth mentioning that a simulation of these proposed designs and numerical algorithms will not be conducted referencing the aforementioned research on SOC implementations which could be generalized to many system designs. All of these topics were examined for how they pertain to the integration of the CubeSat Lunar GPS. Finally, this research can be used to motivate a governing document or design proposal for future engineering, simulating, and testing to develop a CubeSat lunar GPS.

2. GLOBAL POSITIONING SYSTEM INTRODUCTION

2.1 Background

New Global Positioning System (GPS) technology has recently gained the ability to locate one's position within less than tens of meters anywhere on the planet [9]. How this feat is accomplished is by means of a mathematical method called trilateration. The conventional mathematical method calculates pseudoranges of the satellites via the distance equation, then these pseudoranges can be linearized to numerically trilaterate the satellites' and receiver's position [3].

2.1.1 What The Global Positioning System Is

GPS is defined as a satellite based navigation system, where navigation simply means to determine one's position and/or heading [13]. This information can be as trivial as how to get from one's house to the shopping mall, or as indispensable as how an airplane pilot navigates a plane from airport to airport. With GPS, position, velocity, and time (PVT) of the satellites and the user(receiver) can all be determined. GPS is currently open to military and civilian users. The military's GPS is accurate down to the millimeter, whereas the civilian is accurate to the tens of meters [1]. The civilian version is less accurate because of security reasons (Ie. national security) [2].

2.2 Global Positioning System Segments Overview

There are three segments in GPS space, control, and user. Each segment corresponds to a particular area of the GPS. The space segment is the actual constellation of satellites that orbit the Earth. GPS is actually a passive system since the satellites send signals down to a receiver, and the receiver does not send any signals back to the satellites [1]. Next, is the control segment. The control segment ensures the health and status of the satellites [1]. For example, maintaining the satellites' orbits, keeping their clocks accurate, making sure the batteries are charged, and other such satellite systems. This control segment is made up of monitoring stations, ground antennas, and the master control station [1]. All of these are ground based stations that monitor and maintain the satellites, and periodically send corrections and updates. Lastly is the user segment. This segment is the actual GPS receiving equipment which processes the carrier and code signals for determining the user PVT [1]. Today, this can be a hand-held receiver, a system inside an airplane, or even on a cell phone.

2.3 Orbital Mechanics

2.3.1 Two Body Problem

The two body problem involves a single body orbiting around another. It does not have to involve the Earth and a satellite, it can involve any planet, moon, asteroid, star, or anything with sufficient gravity, and one satellite (used generally here) orbiting about this mass (hence two bodies). These orbits can be quantified by the ellipse conic section. Although other conic sections can quantify other orbital mechanics,

the ellipse is specifically used for the two body problem for GPS satellites.

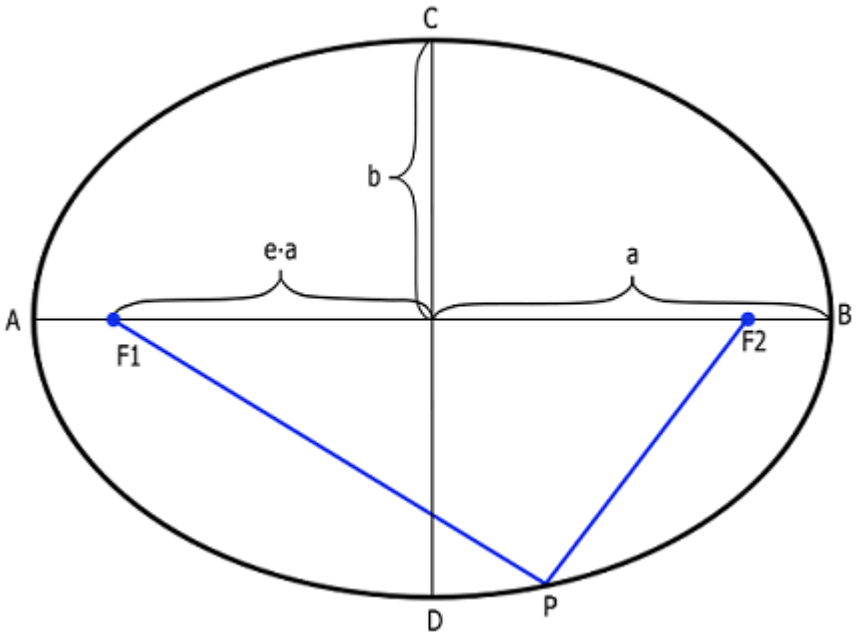

Fig. 2.1: 2D Ellipse [11]

Used Under Creative Commons License

In the above figure an ellipse with its major axis (a) and minor axis (b) are shown. Eccentricity (e) is how elliptical the ellipse is, and ea is the distance from the center of the ellipse to either foci (F1 and F2). Finally, P can be any point along the ellipse, and the distance drawn from the foci to any point can be used to draw the ellipse [11].

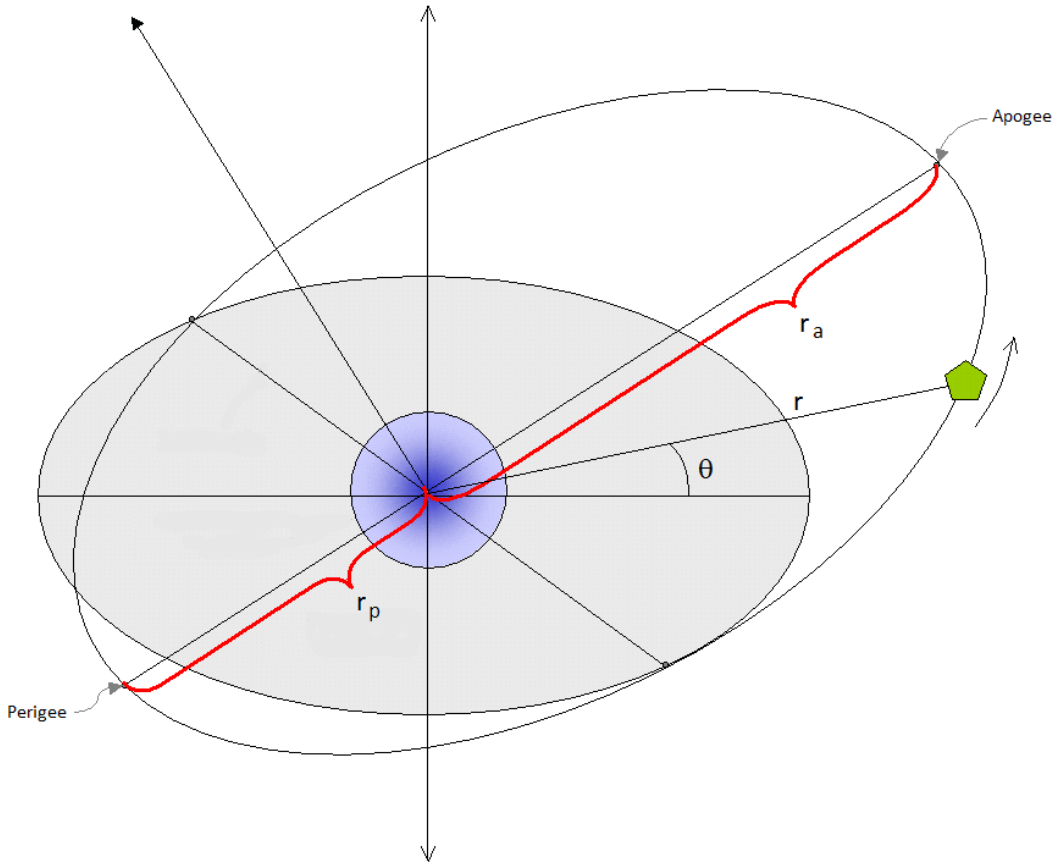

Fig. 2.2: 2D Elliptical Orbital Plane [12]

In this figure, the ellipse has been extended to an orbital plane where the large blue focus is used as the mass being orbited around (assume the Earth), and the angled ellipse represents the orbit of the satellite (with the green pentagon around its edge). The shortest distance from the Earth and the satellite's orbit would be the perigee (r_p). The furthest distance of the orbit would be the apogee (r_a) (There are different terms for this when different common, celestial bodies are involved, however, in general they would be periapsis and apoapsis) [48]. Theta (Θ) is the

angle from a center reference line to a vector (r) from the Earth to the satellite. Another perspective to take with this orbit is in terms of energy. The kinetic energy (KE) would be at its greatest when the satellite reaches perigee. Then, its potential energy (PE) would be at its smallest. The opposite of this would occur when the satellite is at apogee. This also means that the velocity of the satellite is at its highest at perigee, and lowest at apogee.

2.3.2 Orbital Planes

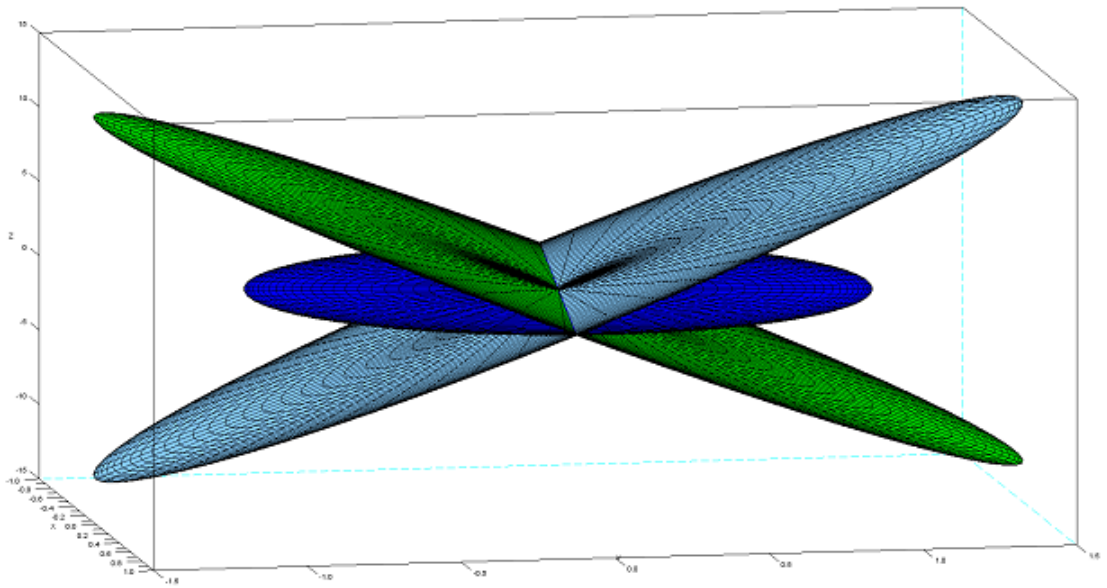

Fig. 2.3: Satellite Orbital Planes

The idea of an elliptical plane can be extended to three dimensions. Consider figure 2.3 above (Note: The cyan and green ellipses have been elongated to illustrate that the orbits are indeed elliptical). The blue plane is the Earth's equatorial plane, and at different angles intersecting it are two orbital planes similar to that of figure

2.2 above. This graphic generated with Scilab is demonstrating each orbital plane with respect to the Earth's equatorial plane. Each satellite could not only be along the edge of an orbital plane, but also in orbit within the plane. For Earth's GPS constellation, there would be a total of six planes, with four satellites per a plane. Finally, this diagram shows where and how the satellites would be with respect to the receiver.

2.3.3 Constellation Design

A constellation is a group of satellites. The orientation of these satellite orbital planes, and their positions within the planes is referred to as constellation design. One important consideration for constellation design is ensuring that the minimum number of satellites for the system to function are visible by the receiver at any given time and position. Another is confirming the planes are not singular with respect to each other or causing many satellites to be singular with each other [2]. The vectors of the satellites or planes become singular when their angles and relative positions approach each other. This causes errors to propagate within the numerical calculations of positions. Referring to figure 2.3 again, it can be seen that each orbital plane is at a sufficiently large angle that these planes are non-singular even close to orthogonal (perpendicular).

The last major component to be considered are the altitudes of the satellite orbits. For Earth GPS, the satellites are at medium Earth orbit (MEO) roughly 20,000km above the Earth. This means the satellites orbit the Earth about twice every 24 hours. This is different than geosynchronous orbit (GEO) where space vehicles orbit

at the same rate that the Earth is spinning (Ie. Spy satellites, ...), and low Earth orbit (LEO) where they orbit several times a day (Ie. International Space Station, Hubble Telescope, ...). The altitude of orbit is important because it ensures that enough satellites will be visible by the receiver.

2.4 Global Positioning System Trilateration Overview

2.4.1 Introduction

How does GPS work? In its simplest form, GPS works by a mathematical method called trilateration. It uses the radii (ranges) of intersecting circles or spheres to determine a location.

2.4.2 2D Trilateration

In order to understand how trilateration works let's consider a two dimensional example. Consider the below diagram (Figure 2.4).

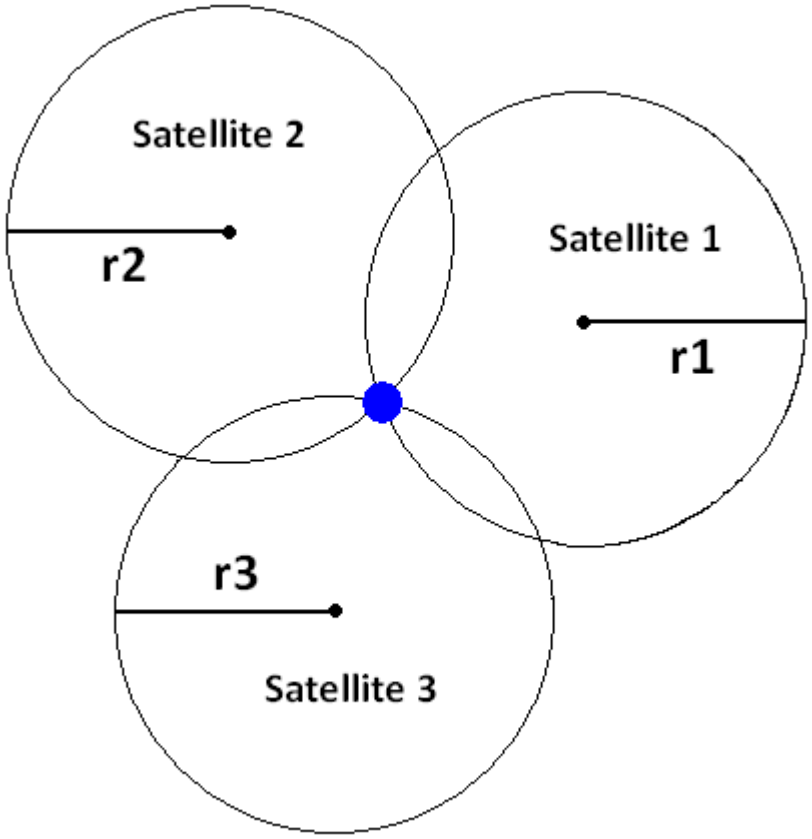

Fig. 2.4: 2D Trilateration

The range of each circle determines the possible distance the receiver is from the origin of that circle. The intersection of each circle narrows the possibility of where the receiver is. So for a 2D plane, three circles are needed to narrow the number of intersections to one, which is the position of the receiver.

2.4.3 2D Trilateration + Error

The above figure and explanation depict how trilateration works under ideal circumstances, however, ideal circumstances do not exist, only practical estimations,

and GPS is no exception. Therefore, errors must be taken into consideration when trilaterating a position. Consider figure 2.5, in this diagram, the blue dot, has been replaced with a region filled with blue. This region illustrates that the user position is not a perfect intersection of all three circles, but an area in the center of the intersection of the circles. This area is proportional to the amount of error created by the error distance of the radius of each circle [1].

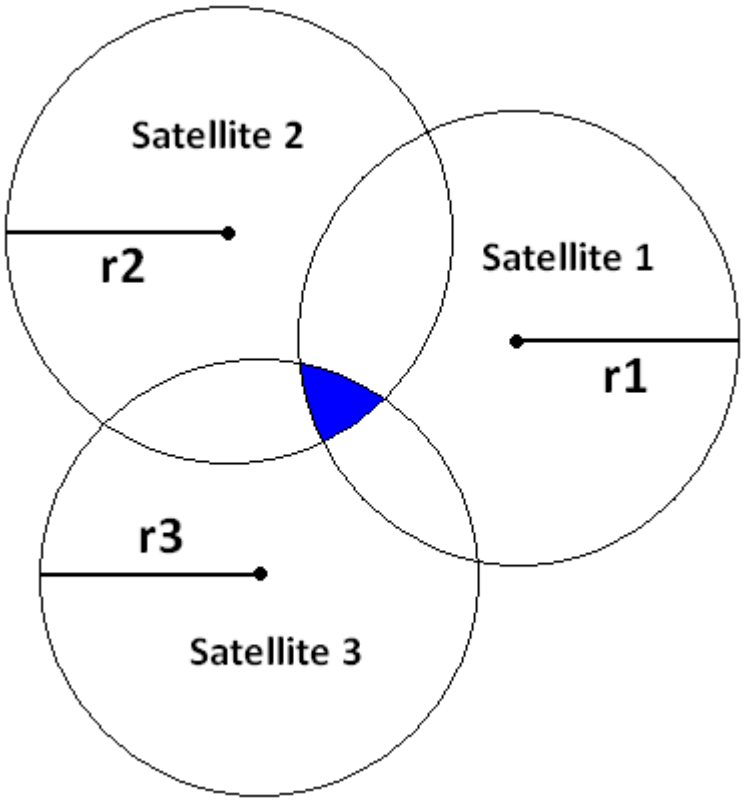

Fig. 2.5: 2D Trilateration + Error

2.4.4 3D Trilateration

Next, take what is known about 2D trilateration, and extend it to 3 dimensions. Again, consider the below diagram (Figure 2.6).

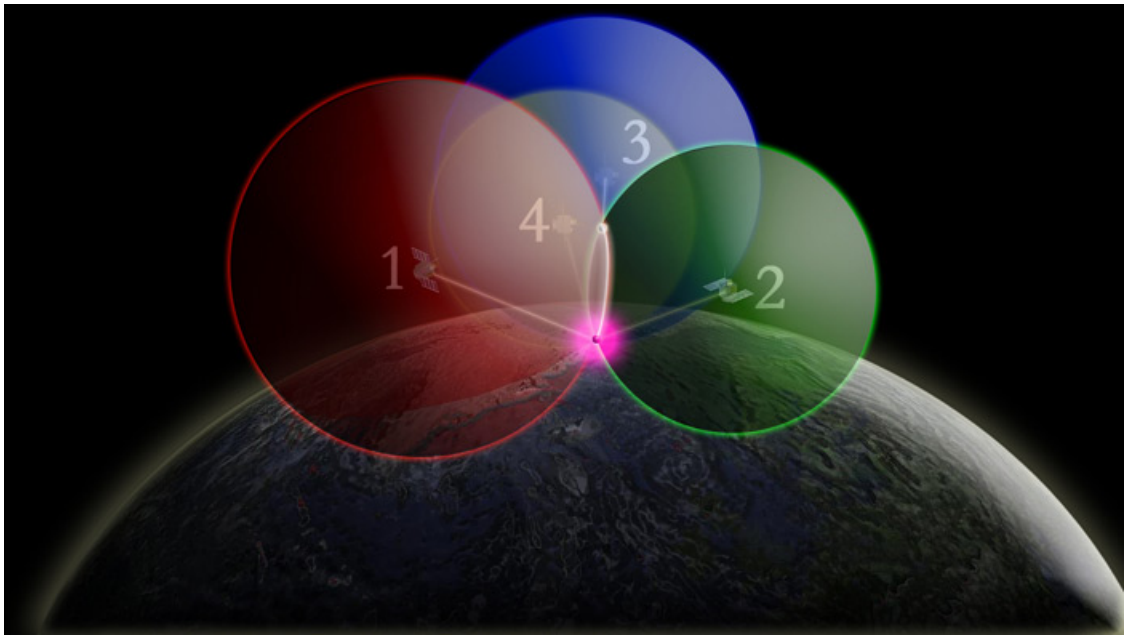

Fig. 2.6: 3D Trilateration [40]

Notice the rings that are formed from the intersection spheres. Also, notice the two dots where the spheres intersect. Since there is a third dimension, another sphere is needed to eliminate the extraneous intersection point. One could add an extra satellite, or simply use the Earth as the fourth sphere. (Note: A fourth satellite is shown in this figure. As it will be discussed later, GPS requires four satellites for pseudorange calculation: x, y, z, and time. Moreover, for accurate z-positioning, the fourth satellite is required).

2.5 Signals

2.5.1 Introduction

There are two primary signals that are transmitted from the satellites. These are the carrier and code signals. The carrier wave is used for carrying the code wave. The code wave holds the data that is sent from the satellite to the receiver such as ephemeris satellite positions, satellite time, and other additional information. The code is modulated onto the carrier for transmission.

2.5.2 Carrier Wave

There are two carrier frequencies under the legacy GPS system which will be explained shortly (Note: There are other carrier and code signals under the modernized GPS, but for explanation purposes only the legacy will be presented since it is the same concept). There is a primary L1 frequency at $154f_0$ MHz, and a secondary L2 frequency at $120f_0$ MHz, where f_0 is the nominal frequency seen by the receiver at 10.23MHz [1]. The reason there are two carrier frequencies is to compensate for the delays created by the Earth's ionosphere through pseudorange differencing [1]. More on ionospheric errors will be covered in chapter five.

2.5.3 Code Wave

The code signal is generally called the pseudorange number (PRN) code which can be either the course/acquisition (C/A) code, or the precision (P) code. The C/A code is a short wave code repeated every millisecond, and is available for use by the military and civilians [1]. The P code is a long wave that repeats once a week. This code

is encrypted, and is only used by the military or those with Department of Defense (DoD) clearance [1]. The PRN code is the actual signal used for PVT determination. Also, the PRN code consists of data that is transmitted which indicates the satellite's health, power status, ephemeris, and other pertinent information.

2.5.4 Modulation

The PRN code is modulated onto the carrier wave by a method called direct sequence spread spectrum (DSSS) [1]. DSSS is a subset of another modulation method called binary phase shift keying (BPSK) [1]. The DSSS is the product of the carrier radio frequency (RF) wave, the data wave, and the spreading (PRN code) wave. The PRN code is a finite, deterministic (pseudorandom) sequence. This is the sequence that is generated for the C/A or P codes, and is repeated periodically as previously mentioned. Also, this is the code that is replicated on the receiver end for signal acquisition and range measurements.

It is common for more than one DSSS signal to be transmitted from a transmitter at a given time. This is accomplished by the methods of interplexing and signals quadrature phase shift keying (QPSK). The QPSK signal is comprised of two binary DSSS signals which have been added together, and have a phase difference of $\pi/2$ radians (90°) [1]. Interplexing allows a third signal to be sent along the carrier as well. The resulting QPSK signal is the equation below.

$$s(t) = s_I(t)\cos(2\pi f_c t) - s_Q(t)\sin(2\pi f_c t) \tag{2.1}$$

The value f_c is the carrier frequency, and $s_I(t)$ and $s_Q(t)$ are in-phase and quadra-

phase functions respectively, they are defined below [1].

$$s_I(t) = \sqrt{2P_I}s_1(t)\cos(m) - \sqrt{2P_Q}s_2(t)\sin(m) \tag{2.2}$$

$$s_Q(t) = \sqrt{2P_Q}s_3(t)\cos(m) + \sqrt{2P_I}s_1(t)s_2(t)s_3(t)\sin(m) \tag{2.3}$$

The functions $s_{1,2,3}(t)$ are the three DSSS signals, P_I and P_Q are the power levels of the signals. Below is an example QPSK signal [1].

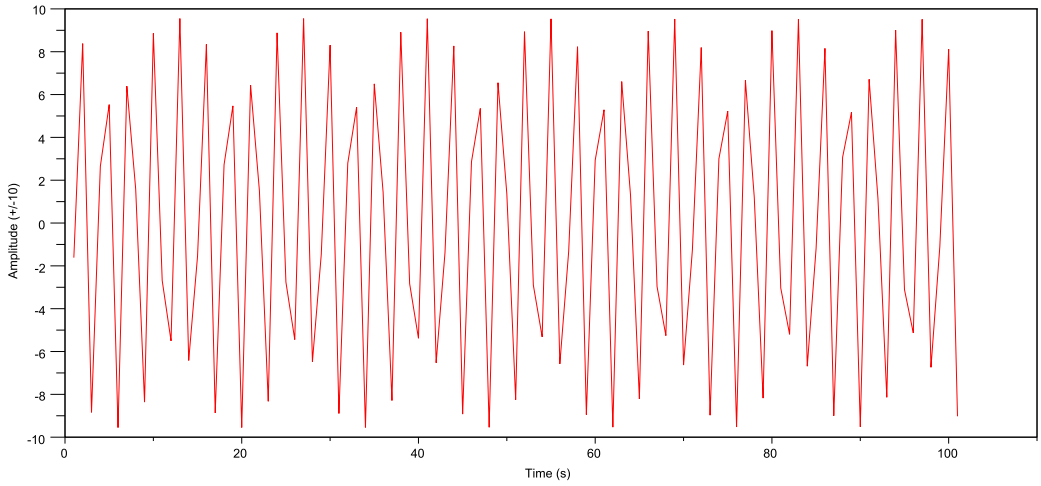

Fig. 2.7: Example Quadrature Phase Shift Keying Signal

2.5.5 Autocorrelation

Since all satellites send their respective carrier signals at the same frequency, and for the receiver to acquire the correct satellite signals, the method of autocorrelation was implemented. The general definition of the autocorrelation function is as follows where $g(t)$ is the desired PRN signal, τ is the phase shift, and T is the chipping period (minimum time interval between transitions for a PRN wave) [1].

$$R(\tau) = \lim_{T->\infty} \frac{1}{2T} \int_{-T}^{T} g(t)g(t+\tau)dt \tag{2.4}$$

This is the function that is used to perform autocorrelation for a desired signal. Autocorrelation is where the receiver phase shifts one signal with respect to another until the two correlate. The next section will explain how this is applied to GPS signals.

2.5.6 Application To Range Measurements

The below figure depicts an example of code replication for autocorrelation. The time t_1 is the time the PRN code signal was sent. Also, starting at time t_1, the receiver was generating a replica PRN code signal identical to the original PRN signal that the satellite transmitted. Once the signal reaches the receiver at time t_2, the receiver begins autocorrelation with the received satellite signal and the replica signal by phase shifting until there is a maximum match. Once the signals match, the Δt is determined by the amount of time that the replica signal was phase shifted. This Δt can be used to calculate the pseudorange.

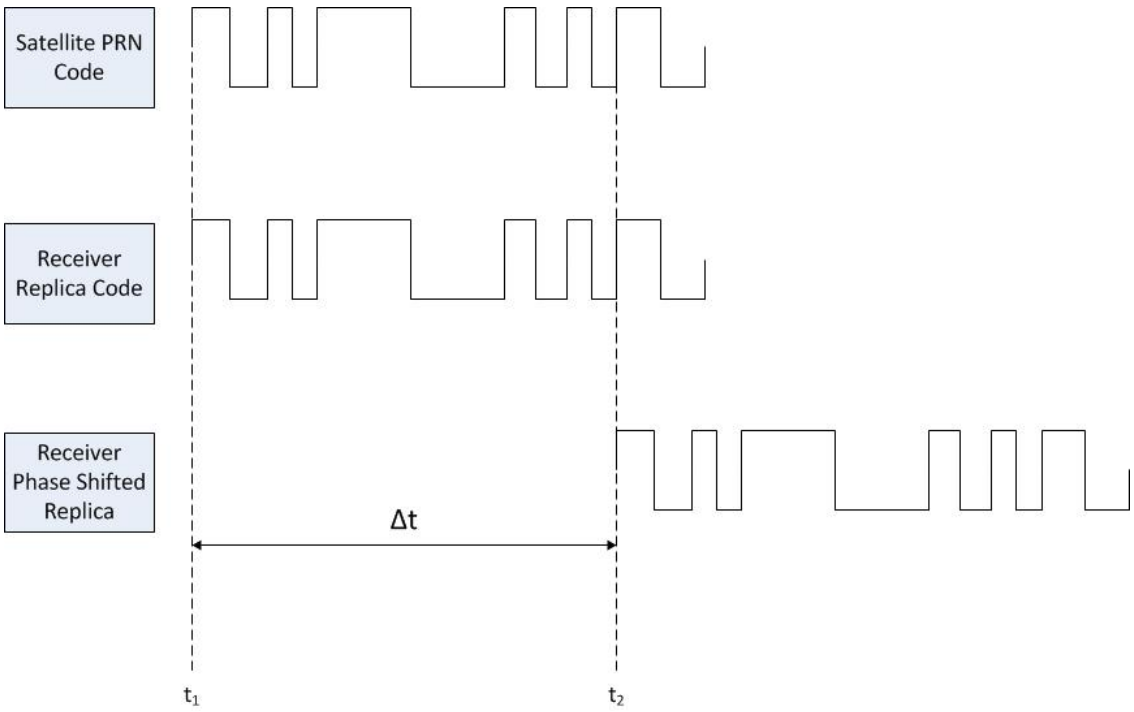

Fig. 2.8: Pseudorange Number Signal Autocorrelation

2.6 Error Correction Overview

2.6.1 Major Causes of Global Positioning System Errors

There are many causes for error within the GPS system. A few of the major reasons are the clock drift from the satellite's on-board clock, relativistic error, and atmospheric effects. The clock drift occurs due to inaccuracies from the atomic clocks on-board the satellites. Although these are supposed to be accurate to the nanosecond (ns), deviations can occur as large as a millisecond (ms). This would result in a pseudorange error of 300km. This is why the control segment monitors these clocks, and periodically sends corrections to them. The Earth's atmosphere causes errors by

affecting the speed of the signal as it is transmitted down to the receiver. Since radio signals are electromagnetic (light) waves, their velocity is subject to being decreased (refracted) by the atmosphere, similar to how visible light is refracted when it passes through a body of water. In turn, this causes errors for the pseudorange measurement since it is based upon the speed of light constant c which is $(3.0\times10^8 m/s)$ in a vacuum, but not when it passes through the atmosphere.

2.6.2 Relativistic Correction

For Earth GPS, both special and general relativity apply. Special relativity applies because the satellites are orbiting the Earth at a high velocity with respect to the receiver, and general relativity applies due to inconsistent gravitational potentials from the Earth. To correct for these relativistic effects, the f_0 frequency is transmitted from the satellites at $f_0 = 10.22999999543$MHz [1]. Relative to the receiver this frequency is 10.23MHz, which is the desired value.

2.6.3 Kalman Filtering

In a nutshell, the Kalman filter is an algorithm for incorporating previous measurements and estimations [1]. This is advantageous for error correction. The Kalman filter works on the principle that the more information one has, the more accurate the estimation will be. It also has the added benefit that it does not require direct measurements or variables [1]. In terms of GPS an example of a direct variable would be the receiver position, and the measurements made would be indirect (ie. pseudoranges). In chapter six, correction of these errors will be discussed in more depth.

2.7 Ranges and Pseudoranges Overview

2.7.1 Introduction

The next question that arises is how to get the ranges of each of the satellites, since one cannot extend a massively long measuring tape to measure the distances. In order to determine the range, one calculates a measurement called a pseudorange [3]:

The equations are below:

$$Geometric\ Range\ (r) = (T_u - T_s)c \tag{2.5}$$

$$Pseudorange\ (P) = r + (t_u - \delta t)c \tag{2.6}$$

where r is the geometric (true) range for a given satellite to the receiver, T_u is the system time when the signal reached the receiver, T_s is the system time when the signal left the satellite, and c is the speed of light constant ($3.0 \times 10^8 m/s$). Since time is in seconds (s), and c is in (m/s), the seconds cancel out, and we are left with meters. This is our measuring tape. However, unlike the geometric range, the pseudorange (P) is not perfect measurement. There are errors that must be considered when calculating it, however, for this example the time offset will only be considered (t_u) which equals the offset of the receiver's time from the system time, and δt which is the offset of the satellite time from the system time (Note: Another way to think of the offsets are how much the satellite or receiver time deviates from the system time) [1].

The below figure helps illustrate the relationship between timing and ranges. The variable meanings are the same as above, along with $T_s + \delta t$ being the satellite time that the signal left the satellite, and $T_u + t_u$ being the receiver time the signal reached

the receiver [1].

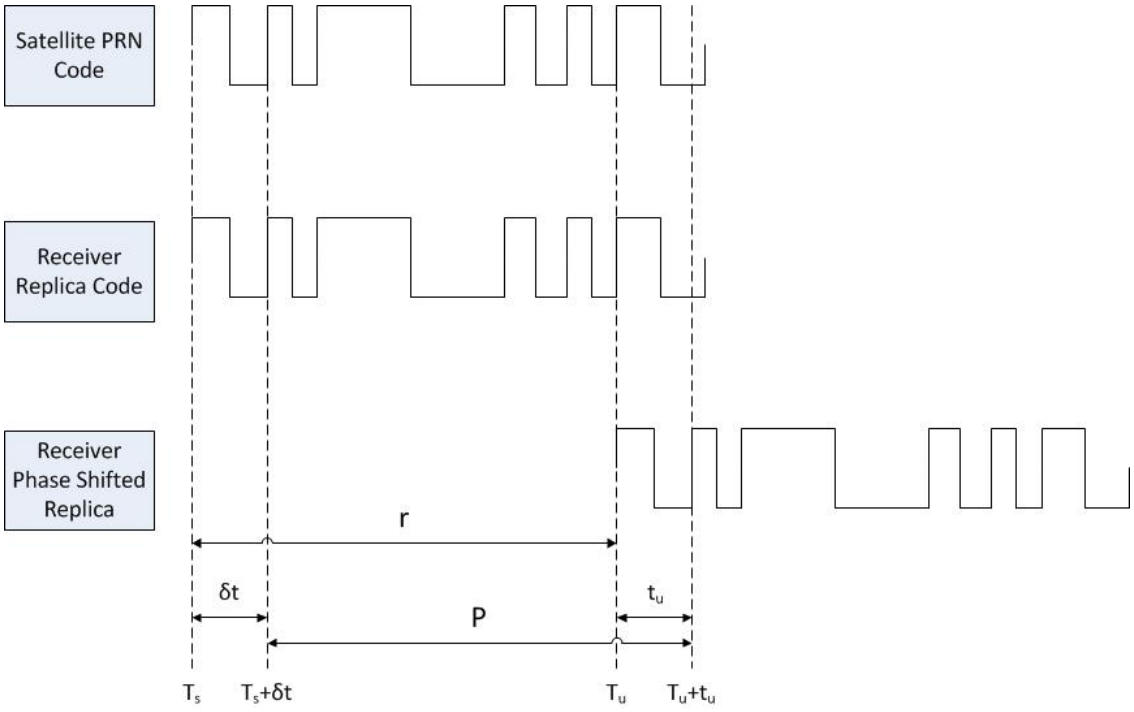

Fig. 2.9: Timing and Offsets For Geometric and Pseudo Ranges

2.7.2 Position Determination

In order to calculate the receiver's position the following method is employed. First, the pseudorange and approximated position are calculated. Next, the difference between actual and estimated position and time is calculated. Finally, we back-solve to determine the actual position and time of the receiver. The equations take the

form of below.

$$x = \hat{x} + \Delta x \tag{2.7}$$

$$y = \hat{y} + \Delta y \tag{2.8}$$

$$z = \hat{z} + \Delta z \tag{2.9}$$

$$t_u = \hat{t_u} + \Delta t_u \tag{2.10}$$

The next section will show how to determine these delta (Δ) values.

2.8 Numerical Global Positioning System Computations

2.8.1 Pseudoranges

Now, to look more deeply into how pseudoranges are calculated, and the errors that are associated with them. The satellites and the receiving stations use cesium or rubidium atomic clocks for their timing, which are accurate down to the nanosecond (ns $= 10^{-9}$). Although this may seem like a very small value, when multiplied by the speed of light our distance error would be 0.1 meters. Moreover, while performing numerical calculations, the errors could easily propagate, especially with ill-conditioned matrices [2]. This is an example of a particular type of timing error referred to as the time bias which is denoted by t_u. Considering the measurements are for distance, the time (T) values will be re-written into the form of a function for each 3D coordinate position (x, y, z). Finally, the pseudorange equation takes on the following form [3].

$$P_j(T_u, T_s) = \sqrt{(x_j(T_s) - x(T_u))^2 + (y_j(T_s) - y(T_u))^2 + (z_j(T_s) - z(T_u))^2} + ct_u \tag{2.11}$$

Below are four satellite plane equations (Note: There would be one equation for each satellite).

$$P_1 = \sqrt{(x_1 - x)^2 + (y_1 - y)^2 + (z_1 - z)^2} + ct_u \tag{2.12}$$

$$P_2 = \sqrt{(x_2 - x)^2 + (y_2 - y)^2 + (z_2 - z)^2} + ct_u \tag{2.13}$$

$$P_3 = \sqrt{(x_3 - x)^2 + (y_3 - y)^2 + (z_3 - z)^2} + ct_u \tag{2.14}$$

$$P_4 = \sqrt{(x_4 - x)^2 + (y_4 - y)^2 + (z_4 - z)^2} + ct_u \tag{2.15}$$

2.8.2 Linearization

The next step to take is the linearization of the pseudorange equation by Taylor Expansion for numerical calculations [3]. Consider the following.

$$P(x, y, z, t_u) \approx P(\hat{x}, \hat{y}, \hat{z}, \hat{t_u}) + (x - \hat{x})\frac{\partial P}{\partial x} + (y - \hat{y})\frac{\partial P}{\partial y} + (z - \hat{z})\frac{\partial P}{\partial z} + (t_u - \hat{t_u})\frac{\partial P}{\partial t_u} \tag{2.16}$$

$$= P(\hat{x}, \hat{y}, \hat{z}, \hat{t_u}) + \Delta x\frac{\partial P}{\partial x} + \Delta y\frac{\partial P}{\partial y} + \Delta z\frac{\partial P}{\partial z} + \Delta t_u\frac{\partial P}{\partial t_u} \tag{2.17}$$

Here we started with the approximated pseudorange calculation $P(\hat{x}, \hat{y}, \hat{z}, \hat{t_u})$, then take the first partial derivative with respect to each coordinate difference. The higher order partial derivatives are simply left off (These would be for additional error corrections such as the aforementioned error).

Now rearrange the change in coordinates [3].

$$\Delta P = \frac{\partial P}{\partial x}\Delta x + \frac{\partial P}{\partial y}\Delta y + \frac{\partial P}{\partial z}\Delta z + \frac{\partial P}{\partial t_u}\Delta t_u + v \tag{2.18}$$

Afterwards, separate the partial derivatives and the changes in each coordinate into

their own matrices, and multiply them together [3].

$$\Delta P = \begin{pmatrix} \frac{\partial P}{\partial x} & \frac{\partial P}{\partial y} & \frac{\partial P}{\partial z} & \frac{\partial P}{\partial t_u} \end{pmatrix} \begin{pmatrix} \Delta x \\ \Delta y \\ \Delta z \\ \Delta t_u \end{pmatrix} + v$$

Here is the successfully, linearized pseudorange equation for one satellite.

Calculating Partial Derivative For Coordinates [4]

$$\frac{\partial P_j}{\partial w} = \frac{w_j - \hat{w}}{\rho_j} \quad w = \text{any coordinate} \tag{2.19}$$

$$\rho_j(T_u, T_s) = \sqrt{(x_j(T_s) - x(T_u))^2 + (y_j(T_s) - y(T_u))^2 + (z_j(T_s) - z(T_u))^2} \tag{2.20}$$

Although equation (2.11) above works great for one satellite, it is not in its most useful form until it can handle all the satellites needed in a view plane [3].

$$\begin{pmatrix} \Delta P_1 \\ \Delta P_2 \\ \Delta P_3 \\ \vdots \\ \Delta P_m \end{pmatrix} = \begin{pmatrix} \frac{\partial P_1}{\partial x} & \frac{\partial P_1}{\partial y} & \frac{\partial P_1}{\partial z} & \frac{\partial P_1}{\partial t_u} \\ \frac{\partial P_2}{\partial x} & \frac{\partial P_2}{\partial y} & \frac{\partial P_2}{\partial z} & \frac{\partial P_2}{\partial t_u} \\ \frac{\partial P_3}{\partial x} & \frac{\partial P_3}{\partial y} & \frac{\partial P_3}{\partial z} & \frac{\partial P_3}{\partial t_u} \\ \vdots & \vdots & \vdots & \vdots \\ \frac{\partial P_m}{\partial x} & \frac{\partial P_m}{\partial y} & \frac{\partial P_m}{\partial z} & \frac{\partial P_m}{\partial t_u} \end{pmatrix} \begin{pmatrix} \Delta x \\ \Delta y \\ \Delta z \\ \Delta t_u \end{pmatrix} + v$$

Finally, here is the equation in the linear $b = Ax + v$ form. Once in this form the x vector can be solved for by most linear least square methods (Note: Most dense matrix methods should be used such as QR factorization, Modified Gram Schmidt, etc... since this will be a dense matrix no bigger than four columns) [2]. Upon solving for the x vector, these delta values can be used to back-solve for the actual receiver

position (Note: For a velocity estimation, take the derivative of the user's position with respect to time).

3. LUNAR SATELLITE CONSTELLATION

3.1 Constellation Orbit Determination

In section 2.3.3 a brief explanation to satellite constellations was introduced. In this section the high level design for the lunar GPS constellation will be further explained. Satellite constellations are based upon several factors including the requirements of the system and their orbital parameters. The requirements of the system may include whether constant signal visibility with the satellites are needed. Another could be if worldwide coverage is required. These constraints determine the number of satellites in a constellation and the altitude of their orbits.

3.1.1 General Constellation Design Theory

The general requirements for a GPS constellation design are as follows [46]:

1. For PVT determination at least four satellites must be visible at all times anywhere in the world assuming worldwide access is required.
2. The position offsets of the visible satellites need to be such that there pseudoranges with the receiver are as non-singular as possible.
3. The amount of updates from ground based station needs to be kept to a minimum.
4. There needs to be a balance between orbital altitude and transmitter power for

the signal.

5. There needs to be a certain level of redundancy in the event of failures.

Considering point 1, one can get away with three satellites if only position determination is necessary, but as stated before PVT determination requires four satellites. Furthermore, considering point 5 for redundancy, the number of visible satellites should be six according to Kaplan and Hegarty [1, 46]. Point 3 is important because if a trajectory needs to be updated, then this requires power and fuel consumption. The fourth is imperative, and additional research will need to be conducted to develop an antenna and transceiver for this subsystem.

3.1.2 The Lunar Global Positioning System Constellation Design

Originally, two constellation designs were considered. The first would have been derived from the GPS currently functioning for Earth, specifically the altitude of the satellites. The second was that the constellation and orbital parameters would have been at a lunar synchronous orbit. Although, the orbital altitude of the lunar synchronous orbit would have been ideal, since relativistic errors and the number of required satellites would have been to a minimum, this altitude (8.7×10^4 km) is too high above the L1 Lagrangian point which is roughly 6.3×10^4 km above the moon [49, 50, 51]. This would have caused the satellites to be pulled back by the Earth's gravitational field. Also, even though the altitude for the Earth-based constellation (5.4×10^4 km) is below the L1 point, it would be too close to it causing the circular orbit to perturb, which would have greatly increased the orbital complexity.

The GPS constellation design in this thesis uses the same aforementioned require-

ments to govern the specific needs for the lunar system. Also, there are the additional specific requirements [46].

1. The satellites should have as close to circular orbits as possible.
2. There should be global coverage of the moon.

Next, several major factors need to be determined for the constellation's design [46].

1. The minimum number of satellites to cover the moon.
2. The minimum number of satellites to determine the user's PVT on the moon.
3. The optimized orbital parameters for the constellation.
   (a) The time it takes for the satellite to orbit around the moon.
   (b) The shape of the orbit.
   (c) The altitude and inclination.
   (d) The number of orbital planes to be used.
4. The signal transmitter power.
5. The optimal level of redundancy.

As it can easily be seen, all of these factors will depend heavily on the requirements of the system. In addition, there is no single correct answer or method to determine these factors. However, there are optimal parameters and conditions for a particular set of design requirements (Note: There can be multiple versions of these as well considering system trade-offs). Next, to analyze the points above specifically for the design proposed in this thesis. First, there is a relation between points one and two where one can be thought of as a subset of two. This is generally because the minimum number of satellites to cover the planet is related to how many are visible at

a given time from a specific position on the planet. Since this number is usually less than the minimum number of four visible satellites for GPS, then this is why it is a subset. Next, point three modifies the first two, because those parameters are used to determine the minimum number of satellite coverage. Point four affects 3.3 because the more powerful the transmitter, the higher the satellite altitude can be. Finally, point five is important because although to create redundancy one simply needs to place more satellites or planes in orbit, however, placing too many extra satellite is not only costly, but if the number of satellites is too large, they can cause singularity to rise in the pseudorange vectors causing errors to grow in the PVT measurements. Therefore, an optimal number of redundant satellites needs to be calculated [46]. In the following section, the determination of the requirements and factors will be shown.

3.2 Satellite Coverage Determination

3.2.1 Line of Sight

Considering satellites transmit their signals in concentrated bands of energy, therefore, direct line of sight is required for signal acquisition to and from the satellites and the receiver. It is obvious that there are a limited number of visible locations where a receiver can be at a given time with correspondence to the position of a satellite. For instance, a receiver at the south pole does not have line of sight with a satellite in position orbiting above the north pole.

3.2.2 Rider Constellation

Since line of sight is a pivotal requirement, this is used to determine the minimum number of satellites that need to be orbiting within a given orbital plane in order to have line of sight coverage (from here on out referred to simply as "coverage"). One such method that is employed to calculate this minimum number is referenced from Rider on using inclined circular orbits [15, 46]. Consider the equation below.

$$\cos(\theta + \alpha) = \frac{\cos\alpha}{1 + h/r} \tag{3.1}$$

Then, solving for the θ gives the following equation:

$$\theta = \arccos\left(\frac{\cos\alpha}{1 + h/r}\right) - \alpha \tag{3.2}$$

where θ is the angle of the body, α is the elevation angle, h is the orbital altitude of the satellite(s), and r is the radius of the body, in our case the moon. Afterwards, θ can be used to solve for the number of satellites, giving the second Rider equation [1, 46]:

$$\cos\theta = \cos c\left(\cos\frac{\pi}{s}\right) \tag{3.3}$$

where c is a parameter that is defined by Rider as a relation between s and θ [1, 46]. Then solving for s gives the number of satellites.

$$s = \left\lceil \frac{\pi}{\arccos\left(\frac{\cos\theta}{\cos c}\right)} \right\rceil \tag{3.4}$$

The reason for taking the ceiling of this equation is to ensure we get an integer value for the satellites since there cannot be a fractional value of a satellite. Next, the number of satellites for GPS purposes can be determined. First, the orbital altitude of the satellites needs to be determined. In order to do this, Kepler's third law was used [26, 46]:

$$\frac{t^2}{r^3} = \frac{4\pi^2}{Gm} \tag{3.5}$$

where t is the orbital period, r is the orbital radius, G is the gravitational constant, and m is the mass of the body being orbited. Finally, solving for r and subtracting the moon's radius yields the satellite altitude.

$$r = \sqrt[3]{\frac{Gmt^2}{4\pi^2}} \tag{3.6}$$

$$sat_{alt} = r - r_{moon} \tag{3.7}$$

In the next section, this equation and the Rider method will be used to calculate the satellite altitude.

3.2.3 Rider Constellation Using Inclined Circular Orbits

To determine the minimum number of satellites for the proposed constellation using the Rider method, a program was written in Scilab to test various orbital altitudes. The graph below shows the results of the minimum number of satellites for coverage on the moon at these altitudes.

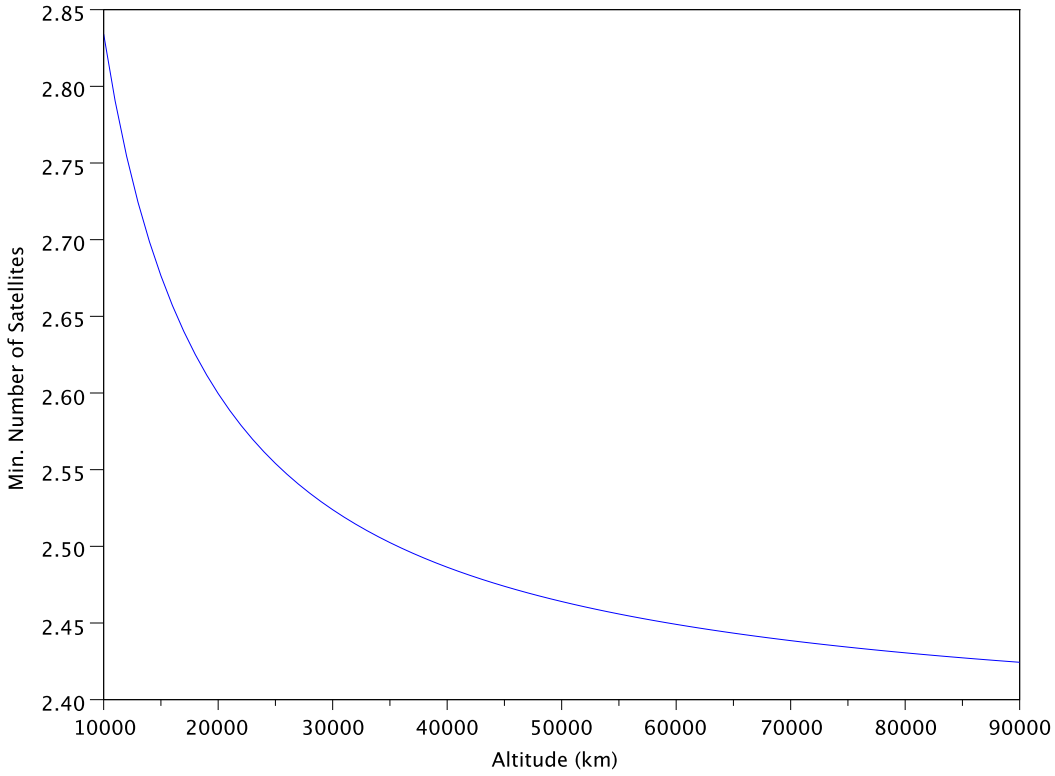

Fig. 3.1: Minimum Number of Satellites For Moon Coverage Using Rider's Method of Inclined Circular Orbits versus Orbital Altitude

These results show that as the orbital altitude of the satellites is increased, the minimum number of satellites needed to provide coverage exponentially decays. Once this test was complete, the desired altitude was calculated to be 3.34×10^4km using Kepler's third law. This altitude was determined by choosing an orbital period equal to that of one-fourth of a moon day which equals 6.8305 Earth days. Again, it was desired to have the satellites in a lunar synchronous orbit where they would orbit the moon at the same rate it rotates (27.322 Earth Days), or with an orbital

period equal to half of the moon's rotation period similar to that of the Earth's GPS altitude [9, 46]. However, this would have caused the satellites to have an orbital altitude of 8.7×10^4 km which is higher than the L1 Lagrangian point (6.3×10^4 km) for the synchronous orbit which would have caused the satellites to be pulled in by the Earth's gravity [49, 50, 51]. As for the half moon period orbit, with an altitude of 5.4×10^4 km the satellites would have been too close to the L1 point causing the orbits to become unstable.

Once the altitude was determined, it was used to calculate the minimum number of satellites per plane. Referring back to Figure 3.1, using the calculated altitude the minimum number of satellites to cover the moon would be approximately 2.5 satellites per plane [46]. Now if this design was simply for having coverage by at least one satellite, then taking the ceiling of this would give us three satellites per plane totaling six satellites. In the aforementioned sections GPS was shown to require more satellites. Therefore, a minimum coverage of at least three visible satellites anywhere on the moon calculates to 7.5 satellites per plane totaling 15 satellites (Note: One plane would have one less satellite, or to make it even there could be 16 satellites), four satellites for minimum PVT would be 10 satellites per plane totaling 20 satellites, and a coverage of at least six satellites (two extra for redundancy) would be 15 satellites per plane, with 30 satellites in total [46].

3.2.4 Estimated Path Loss

Elaborating on point 4 from section 3.1.2, the transmitter power needs to be related to the orbital altitude that was calculated above. There are two factors that affect the

altitude regarding transmitter's power. The first is that there is very limited power and space within the CubeSat, so a larger, more powerful transmitter cannot simply be installed. The second is if the receiver is not able to detect a strong enough signal from the satellites at an altitude of 3.34×10^4 km, then a lower altitude will have to be selected. Since it is beyond the scope of this thesis to fully research and engineer the transmitter, a rough order of magnitude estimate will be calculated.

The basis for this estimation is that the free space path loss must be less than the maximum allowable path loss [22]. What this means is that the amount of signal lost during transmission (signal propagation) cannot be below the minimum threshold of power required for the receiver to detect the signal [22]. What dictates this is the inverse-square law as stated below:

$$p = \frac{1}{r^2} \tag{3.8}$$

where p is the power, and r is the radius or distance of the transmitted signal. The inverse-square law for electromagnetic (radio) waves is for every unit distance that the wave travels, the unit area that the wave covers is the distance traveled squared. This also means that the power of the signal drops at a rate inversely proportional to this effective area squared.

Next, in order to provide a basis as an estimate for the maximum allowable path loss, the weakest signal power that can be detected is referenced from the Galileo GPS specification which is -157 dBW for the L1 band signal [1]. This power rating can be converted into watts using the following equation:

$$P_{dBW} = 10log_{10}P_W \tag{3.9}$$

$$P_W = 10^{\frac{P_{dBW}}{10}} \tag{3.10}$$

where P_{dBW} is power in decibel watts and P_W is power in watts. The value after converting -157 dBW into watts is 2.0×10^{-16} W. This is a very small power signal, however, it is not uncommon for the order of magnitude for the amount of power that is detected by the receiver [22]. Next, the signal's power at the receiver is related to the transmitted power of that signal by the path loss [1].

$$P_r = \frac{P_t G_t G_r}{\Lambda} \tag{3.11}$$

In this equation, P_r and P_t are the power levels of the signal at the receiver and transmitter respectively, G_r and G_t are the signal gains from the antennas connected to the receiver and transmitter, and Λ is the path loss of the signal [1]. What is wanted here is the path loss, and below is the equation for Λ.

$$\Lambda = L\left(\frac{4\pi d}{\lambda}\right)^2 \tag{3.12}$$

The values d and λ should be familiar, they are the distance of the transmitter and receiver, in our case, it is the orbital altitude of the satellite, and λ is the wavelength of the signal defined by $\lambda = \frac{c}{f}$ where c is the speed of light, and f is the frequency of the signal [1, 26]. Now, L is the propagation loss caused from various factors such as signal degradation, obstacles in the path of the signals, and attenuation [1]. Another perspective of L is that it is the error term. A program was written in Scilab using

frequencies starting at 400 MHz up to 1.6 GHz in 50 MHz increments, and their respective wavelengths were calculated, in order to calculate the possible path losses. Also, the orbital altitude of 3.34×10^4 km was plugged into the program. The results can be seen in the graph below.

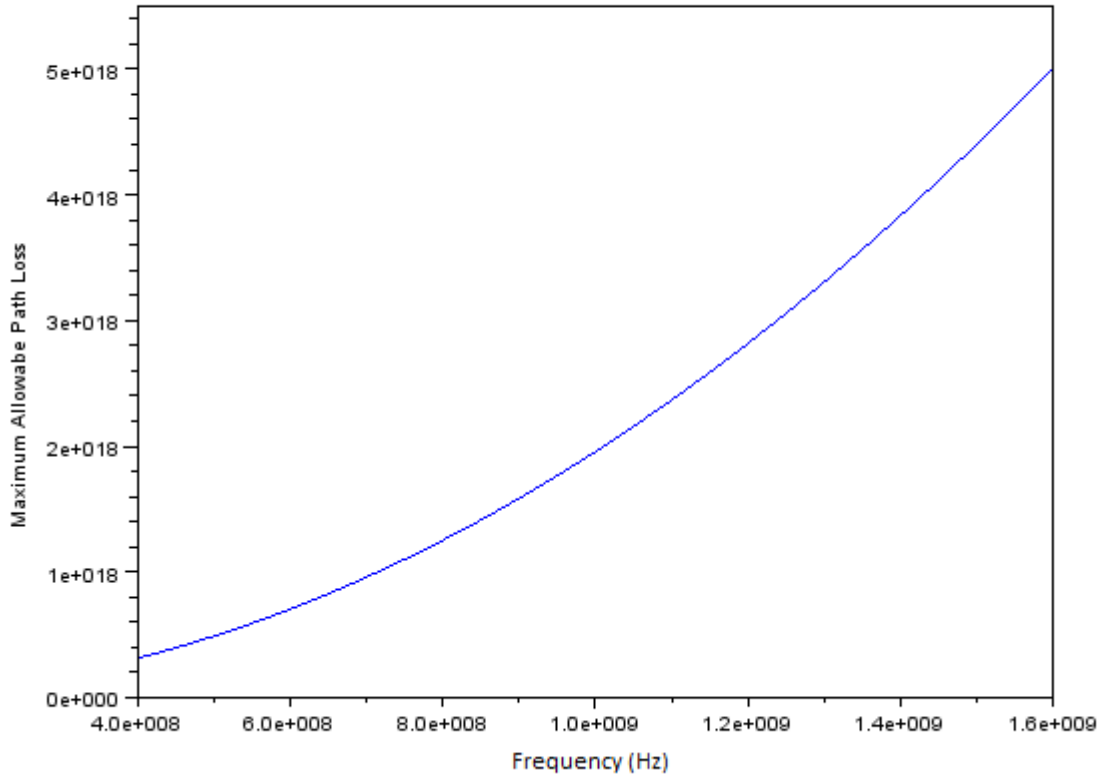

Fig. 3.2: Maximum Allowable Path Loss versus Frequency

If we consider Λ in this graph to be the maximum allowable path loss, then the free path loss must stay below this curve [22]. This gives a good, estimated constraint for the transceiver to be installed in the CubeSat. This graph also shows that the

higher the chosen frequency the more powerful the transmitter must be. Finally, the rationale for this range of chosen frequencies is because the current L1 carrier frequency for GPS is 1.575 GHz for the high range on the graph, and the low range is because there were ultra high frequency (UHF) radio transceivers found for CubeSat which start at around 400 MHz [1].

3.3 Lunar Gravitation Abnormalities

The last major aspect to consider for the satellite orbits deals with the influence of the moon's gravitational field abnormalities. As discussed in the orbital mechanics section of this thesis, orbits are elliptical in shape. However, all orbiting bodies have perturbations of their orbits. This can be caused from the gravitational forces of other bodies acting upon them. For instance, the sun's gravity also affects the moon's orbit even though the primary body acting on the moon is Earth. Furthermore, research has been conducted by NASA showing the perturbations of space vehicles orbiting the moon [23]. The results of this research indicate that what causes the perturbations of satellites in lunar orbit is from the moon having lunar lava that has different mass than the rest of the moon [23]. These are called "mascons", short for mass concentrations because the mass of these areas is so great, that it causes these gravitational perturbations [23]. Therefore, the possibility exists that CubeSats may be sensitive to these perturbations due to their small mass, however, the high altitude proposed in this thesis, may help to alleviate some of the gravitational perturbations from the mascons.

These perturbations and trajectory drifts need to be compensated for. For in-

stance, if these go unchecked, the satellites may drift closer to one another causing singularity of the pseudorange vectors, and thereby increasing the possibility of error measurements. Furthermore, the satellites can possibly even drift out of their respective orbital planes which would render the system useless, or even crash into the moon, as what happened towards the end of the Apollo 16 mission [23].

In order to correct for these perturbations or any other trajectory drift, there will need to be something that can generate a force to accelerate the satellite in order for its trajectory to be corrected. However, per the CubeSat specification, neither propellant nor any pyrotechnics are allowed, so a typical, propellant driven thruster or reaction control system (RCS) will not be permitted [24]. Even if this were allowed, it is not feasible to store all the necessary propellant for such a system. One solution to this problem is to use a propulsion system that does not use pyrotechnics. Such a system was developed by Rysanek and Hartmann from the University of Illinois for the Illinois Observing Nanosatellite (ION) [25]. This system uses a vacuum arc thruster (VAT) to produce ionized plasma which provides the specific impulse to propel the satellite [25]. The VAT has a thrust to power ratio of roughly $10\frac{\mu N}{W}$, and produces a impulse of $1\frac{\mu N * sec}{pulse}$ [25]. The VAT draws 1 to 100 watts driven by 5 to 35 volts direct current (DC) [25]. With this system it would be possible to implement it for our specific purposes.

4. LUNAR GLOBAL POSITIONING SYSTEM SEGMENTS

4.1 Overview

As described before in section 2.2, there are three major segments to GPS system segments space, control, and user. First, the space segment includes the satellites and their systems. Secondly, the control segment includes the ground stations that control, track, and maintain the satellites. Finally, the user segment is the actual GPS receiver and its systems. Another perspective of the segments is that this is the high level architecture of the GPS system. In this chapter, the high level architecture for the lunar GPS segments will be covered. Since the focus of this thesis is mostly about the satellites themselves, this is what will be covered.

4.2 The Lunar Space Segment

4.2.1 Requirements

There are only two major requirements for the space segment. The first is to adhere to the aforementioned constellation design in chapter 3. The second is to design this architecture for the CubeSat platform. Even with just these two requirements, the solutions to them are not trivial or exclusive.

4.2.2 The Satellite Platform - CubeSats

The CubeSat platform was designed by California Polytechnic State University, San Luis Obispo, and Stanford University [16]. Their purpose was to develop a pico-satellite (a satellite $\leq$ 1kg in weight) platform and delivery system that was affordable and standardized, yet robust enough for other colleges and universities to begin satellite and space research programs [7, 16].

A major constraint and challenge of this thesis is to keep the hardware to a volume that will fit within the CubeSat architecture. CubeSats are currently designed to dimensions of $1000cm^3$ and 1kg payload constraint with the maximum size being three modules [7]. Therefore, the largest volume allowed would be $10x10x30cm^3$ and up to 1.33kg. The compelling reason for considering the CubeSat platform is that it is substantially less costly than current GPS satellites and has already been flight tested on many missions. Currently, a GPS satellite costs roughly on the order of magnitude of hundreds of millions to billions of dollars to develop and deploy [34]. This is due to the cost of the atomic clock, size, and weight of the satellite. CubeSats, on the other hand, are on the order of tens of thousands to a few million dollars [33].

4.2.3 Satellite Payload

The general payload each satellite would contain are the electronic and computer hardware, the atomic frequency standard (AFS) clock, the transceivers, the battery and power supply, the vacuum arc thruster (VAT), the solar panels, and the chassis. There are multiple kits which can be acquired for designing and building CubeSats. One such kit which is considered in this thesis is the Pumpkin CubeSat Kit [33]. The

pumpkin kit includes: CubeSat chassis, motherboard, pluggable processor module (PPM) processor, bus, and SD/MMC card for data storage [33]. Furthermore, the kit contains various development, testing, and interface hardware, software, and tools for building the CubeSat [33]. The chassis can come in various unit sizes of 0.5U, 1U, 1.5U, 2U, and 3U of the CubeSat dimension specification [33]. Also, the PPM can be used not only to run the base necessities of the CubeSat such as the bus, power distribution, satellite health, etc..., but can also be used to run some GPS specifics.

Additionally, there are satellite specific subsystems which would be the attitude and orbital control system (AOCS), the telemetry, tracking and control (TT&C), the communications units, and the navigation data unit (NDU). The AOCS controls the relative orientation (attitude) of the satellite, orientation of its solar panels, and also performs various maneuvers such as yaw, pitch, and roll of the satellite [34]. This system would interface with the VAT to perform these maneuvers specifically when an attitude or orbital trajectory is sent from the control segment. The TT&C is where the satellite tracking, navigation, and ephemeris data acquisition from the control segment occurs [1]. The NDU is the main system controller. This is where the data received from the TT&C would be stored, and where the PRN codes would be generated [1]. The NDU also interfaces and controls the various satellite subsystems [1]. Lastly, the communications system would handle the signal modulation between the PRN codes and the carrier signals [1].

The PPM will not be able to handle all of these systems, but due to size constraints, each module will not be able to be implemented individually. For the additional hardware to control, interface, and integrate these systems a viable option would be

to use a field programmable gate array (FPGA). Furthermore, the FPGA could be used to control other GPS related aspects such as the AFS, and any other subsystem that may be required. Finally, with the volume restrictions, current AFS' cannot be used, and in the next section this will be addressed.

4.2.4 A New Atomic Frequency Standard

Quite possibly the largest hurdle that needed to be overcame was determining a suitable AFS that would fit within a CubeSat. All satellites use an AFS to ensure a reliable clock frequency to reference. However, these are usually large, heavy, and expensive. Recently, there has been much advancement with this technology, and now there has been developed chip-scale atomic clocks (CSAC) which are roughly $10mm^3$ in volume, and consume only 30 mW [19], making it suitable for an embedded design. In addition, the proposed CSAC has a Allan Deviation less than 1×10^{-11} [19].

The CSAC works by coherent population trapping (CPT) [18, 19]. To fully understand all of the intrinsic details of CPT, a full introduction into quantum mechanics and physical chemistry would be required. Since this is beyond the scope of this thesis, only a brief overview of CPT will be presented in application to the CSAC. CPT essentially occurs when an alkali atom is excited into a higher energy state [32]. An alkali cell is filled with barium hexanitride (BaN_6) and rubidium chloride (^{87}RbCl) which react to form their respective, pure elements barium, nitrogen, chlorine, and what we desire rubidium (^{87}Rb) [18]. Next, the rubidium vapor is excited from its ground state ($5S_{1/2}$) to the next excited state ($5P_{1/2}$) by emitting two vertical-cavity surface emitting lasers (VCSEL) [18]. After this excitation process, a resonance light

is emitted which can be measured by a photo-detector [19]. Then, from the detector, an electronic circuit such as a phase locked loop (PLL) can lock onto the electronic signal sent from the detector producing a stable reference frequency [19].

In the CSAC designed by J.F. DeNatale, R.L. Borwick, et. al, they used voltage controlled crystal oscillator (VCXO) running at 569 MHz to drive an injection locked oscillator running at 3.4 GHz instead of a typical PLL and voltage controlled oscillator (VCO) to control and stabilize the physics package [19]. Their rationale for switching from the PLL is that it decreased the power consumption from a total of roughly 43mW to below 15mW for the control electronics [19].

Using the CSAC as an AFS for the CubeSat appears to be advantageous for our requirements since it is small and low-powered. The last critical aspect to consider is if the CSAC is stable. One of the standards for determining clock stability is the Allan Deviation [1, 35]. The equation below is for the Allan Variance:

$$\sigma_y^2(\tau) = \frac{1}{2}\langle(\Delta y)^2\rangle \tag{4.1}$$

where τ is the time sampling period, and $\langle(\Delta y)^2\rangle$ is the average of the difference in samples (y) [35]. Then, if we take the square root of the Allan Variance the results is the Allan Deviation $\sigma_y(\tau) = \sqrt{\sigma_y^2(\tau)}$.

Since the CSAC and current AFS' use (^{87}Rb), and referencing the Galileo GPS specification and the Allan Deviation, the clock validity time can be estimated given a desired distance tolerance [1]:

$$t = \frac{d_{error}}{\sigma_y(\tau)c} \tag{4.2}$$

where $\sigma_y(\tau)$ is the Allan Deviation, c is the speed of light in a vacuum, d_{error} is the allowable distance error, and t is the amount of time that can elapse before a clock update needs to be sent to the satellite from the control segment before the distance error grows past its tolerance. Using this equation, the time for update was estimated applying the data from the studied CSAC [19]. Assuming a distance tolerance of ten meters, the time for an update would be over 55 minutes and 30 seconds. This time is a little short, but definitely manageable. If the distance tolerance is extended to 50 and 100 meters, the time for update is a little over approximately 4 hours and 30 minutes, and approximately 9 hours and 15 minutes respectively. Finally, a more in depth discussion on clock drift will be presented in the next chapter.

5. LUNAR POSITION, VELOCITY, AND TIME DETERMINATION

In chapter two, the basics of position determination using pseudoranges was introduced. Within this chapter, a more intensive explanation of PVT determination will be presented along with error corrections. Moreover, these topics will be applied to the proposed lunar GPS using the constraints of the CubeSat platform.

5.1 Error Handling

Before diving into PVT determination, error correction will be discussed first. Various types of errors (noise) are present with GPS measurements, however, not all errors that apply to Earth based GPS apply in the same way or at all for the moon. For instance, multipath should be less of an issue, especially for explorers since buildings are not present on the moon. However, as colonization begins, or areas near mountainous regions, craters, and canyons, multipath errors will become more common. Also, errors created by gravitational disturbances from the oceans and tides will obviously not be of concern since they do not exist on the moon. The errors which will be similar between the Earth and the moon are ephemeris, atmospheric, noise, relativistic, hardware, and clock [1, 27]. Of course, there will be differences in the specifics for these errors, yet the concepts will be the same.

To begin, consider again the pseudorange equation from chapter two.

$$Pseudorange\ (P) = r + (t_u - \delta t)c \tag{5.1}$$

Next, to add the error term in terms of the time difference:

$$Pseudorange\ (P) = r + (t_u - \delta t + \delta t_e)c \tag{5.2}$$

where δt_e is the sum of all the errors terms as shown below (Note: this was denoted as v in chapter two).

$$\delta t_e = \sum_{i}^{n} \delta t_i \mid i = individual\ error\ terms \tag{5.3}$$

$$= \delta t_{ion} + \delta t_{clk} + \delta t_{rel} + \delta t_r \tag{5.4}$$

The first three errors terms are apparent, and δt_r is the error term for all residual errors not counted in the first three terms, and all other errors such as ephemeris, unknown atmospheric particles, signal noise, hardware, lunar gravitational anomalies, and any other unknown errors [1, 27]. In this thesis only the first three terms will be considered since, these should be the areas that cause the largest amount of errors in the pseudorange.

5.1.1 Relativistic

The first set of errors to be considered will be those of relativity. There are two relativistic effects postulated by Einstein, special and general relativity, and both are of importance to satellites and space vehicles [1, 27, 28]. Special relativity occurs when the speed of an object is different than that of an observer in a different reference frame [28]. Specifically, when the satellite is moving at a different velocity than that

of the receiver (which in all cases the satellites velocity is much greater than that of the receiver) [1, 27]. General relativity occurs when two objects have different accelerations, in terms of orbiting satellites, when there are different gravitational potentials between the satellite and the receiver [1, 27, 28].

Fortunately, to determine relativistic correction, a frequency shift simply needs to be calculated at the satellite's clock [1, 27]. Once this is performed, the receiver will measure the desired frequency [1, 27]. Consider the base frequency ($f_0 = 10.23MHz$) for Earth's GPS from section 2.6.2 with the correction to 10.22999999543 MHz [1]. The receiver will measure f_0 at the desired frequency, while the satellite will send the signal at the relativistic correction frequency. The equation for calculating this is below:

$$-\frac{f_0 - f'}{f'} = \frac{1}{2}\left(\frac{v}{c}\right)^2 + \frac{\Delta U}{c^2} \tag{5.5}$$

where f_0 is the frequency at the receiver's reference frame, f' is the frequency at the satellite's reference frame, c is the speed of light, v is the velocity of the satellite, and ΔU is the difference of gravitational potentials [27]. The $1/2(v/c)^2$ term comes from the special relativity derivation via the Lorentz transformation, relating the velocity of the satellite and the speed of light in its reference frame versus the receiver's frame [28]. The $\Delta U/c^2$ term is from general relativity regarding the change in gravitational potential energy and the speed of light [28]. The difference in gravitational potential with respect to GPS calculation is determined as follows:

$$\Delta U = \frac{G}{sat_{alt} + r_{moon}} - \frac{G}{r_{moon}} \tag{5.6}$$

where G is the gravitational constant for the moon, sat_{alt} is the altitude of the satel-

lites as described from chapter three, and r_{moon} is the radius of the moon [27].

The important concept to understand from this is that of reference frames. There are two reference frames, one for the receiver, and one for the satellite. Per Einstein's postulates the laws of physics and the speed of light must remain the same in all inertial reference frames [29]. These two postulates must hold true regardless of the event occurring in each inertial reference frame [29]. What this means is if the speed of light is kept constant to both the receiver and the satellite in their respective inertial references, then time must change to compensate for the relative motion of the satellite. This is called time dilation [28]. Since the signal travels at the speed of light, the time must change, and since time is inversely proportional to frequency this causes it to shift slightly. It is worth noting that the greater the velocity of the satellite as it approaches the speed of light, the more the frequency must be shifted.

The above relativistic correction is assuming that the orbit is perfectly circular. However, GPS orbits have a slight eccentricity to them, there are some relativistic errors that are related to this [1]. To correct for this the following equation is used:

$$\Delta t_r = Fe\sqrt{a}sinE_k \tag{5.7}$$

where e is the eccentricity of the satellite's orbit, a is the semi-major axis of the elliptical orbit, E_k is the phenomena related to the eccentricity of the orbit, and F is a relativity correction constant equal to $-4.44 \times 10^{-10} s/\sqrt{m}$ [1]. For our purposes $\Delta t_r = \delta t_{rel}$.

5.1.2 Clock Drift

Clock drift is an important error that must be considered with GPS measurements. Furthermore, since a new AFS is being considered, there are innately new errors that arise. Consider the following equation:

$$\delta t_{clk} = b + d_r t + at^2 + \delta t_{rel} \tag{5.8}$$

where b is the clock bias, d_r is the clock drift, a is the clock acceleration or clock aging, and δt_{rel} is the same as the previous section [1, 27]. First, the clock bias is the satellite's clock time skewed from the system time. Second, the clock drift is the rate at which the satellite's clock is changing from the system time. Lastly, the clock aging is the change in rate of the clock drift. The form of this equation should give a resemblance of the kinematic position function ($x(t) = \frac{at^2}{2} + v_0 t + x_0$) [26].

As clock drift errors are applied to the CSAC, in theory, the same corrections should be plausible as if it were any other rubidium AFS. This is not an unreasonable assertion since the Allan Deviation, the standard for measuring timing performance was used for both the CSAC and conventional RAFS.

To look more deeply into these concerns the equation from last chapter which indicated the necessary clock corrections was graphed as a function of distance error.

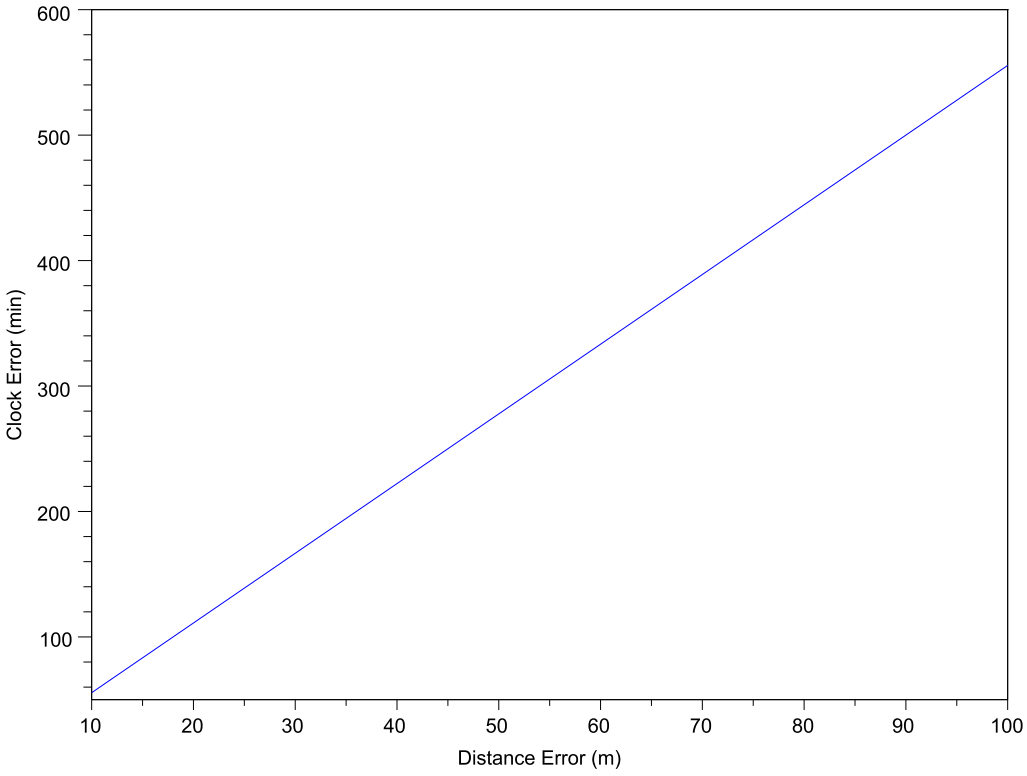

Fig. 5.1: Clock Error versus Distance Error of Chip-Scale Atomic Clock

Setting equation 5.8 equal to equation 4.2, and list as a function gives the following.

$$t = \frac{d_{error}}{\sigma_y(\tau)c} \tag{5.9}$$

$$t(d_{error}) = t \tag{5.10}$$

$$\delta t_{clk}(d_{error}) = t(d_{error}) \tag{5.11}$$

This is essentially the clock offset. Next, take the derivative to obtain the clock drift.

$$\frac{d(\delta t_{clk})}{d(d_{error})} = \frac{1}{\sigma_y(\tau)c} \tag{5.12}$$

This means that the clock drift is a constant in this instance which was expected since the graph shows a linear change in the clock offset. To verify this the change in clock error divided by the distance error can be calculated.

$$\frac{\Delta(\delta t_{clk}(d_{error}))}{\Delta d_{error}} = (\sigma_y(\tau)c)^{-1} \quad \square \tag{5.13}$$

Plugging in the CSAC values for this calculation produces a clock drift of roughly $5.56\frac{min}{m}$ which agrees with the results from chapter four. The other repercussion this results shows is that the clock drift acceleration is constant. This is a somewhat bold statement to imply, albeit a necessary one since it does produce favorable linearity in the numerics. Furthermore, the data from research conducted by Denatale shows their CSAC does have improved stability with time [19]. Therefore, if accounting for clock acceleration does become an imperative issue, there are some options. First, if the acceleration is not large, and sufficiently stable, one can simply add this to the residual errors. The second option is to calculate variances and expected errors using random variables, and so long as these values remain consistent, this would be acceptable. Lastly, if a Kalman filter is being employed, this can help with correcting for these uncertainties. More on Kalman filter will be presented in the next chapter.

5.1.3 Lunar Ionosphere

All atmospheric effects cause errors on signals sent from satellites in the form of refraction. In the case of the moon, it is the ionosphere which may have the largest affects on these signals since the moon does not have much of any other atmosphere(s). According to recent NASA research by T. J. Stubbs, the lunar ionosphere is made up of ionized dust particles which make their way into the lunar air [14, 20, 21]. Dealing

with ionospheric errors and its effect on signals is nothing new here on Earth, but it is different for the moon's ionosphere since it is made up of dust, whereas the Earth's is not. The key concept about ionospheric errors is that of the index of refraction. Refraction occurs when electromagnetic waves change mediums. This causes the wave to slow down, thereby changing its path of travel and distance.

$$c = vn \tag{5.14}$$

The speed of a light wave (c) is given by multiplying the speed of the wave (v) and the index of refraction (n) [26, 27]. One way of looking at the index of refraction is that it is the transformation of the speed of light in a vacuum to the propagation velocity of the electromagnetic wave as it flows through a particular medium. From this the wave velocity and the index of refraction can be solved by simple algebra. Now, there are phase and group waves. The phase waves can be thought of as each individual wave that exist within the total signal. For instance, the carrier and the code waves each are phase waves. The group wave is all the phase waves modulated into one. This means that the velocity of the individual phase waves can be different than the velocity of the group [1]. Applying the above equation produces:

$$c = v_p n_p \tag{5.15}$$

$$c = v_g n_g \tag{5.16}$$

where p and g are phase and group respectively. Next, the group velocity can be calculated in terms of the phase velocity:

$$v_g = v_p - \lambda \left(\frac{dv_p}{d\lambda} \right) \tag{5.17}$$

where λ is the wavelength, and the derivative of the velocity with respect to the wavelength times the wavelength affects the group velocity. Per Xu, a first order estimation of this equation produces it in terms of the index of refraction and frequency [27].

$$n_g = n_p + f\left(\frac{dn_p}{df}\right) \tag{5.18}$$

Next, when applying these general wave equations to the lunar ionosphere, we can determine each index of refraction. First is the one for the phase:

$$n_p = 1 + \frac{e_2}{f^2} + \frac{e_3}{f^3} + ... \tag{5.19}$$

where e_i is a coefficient related to the electron density (amount of electrons in a given area). Second, the equation for the group can be determined by differentiating the above equation with respect to frequency, then plugging it into equation 5.18 [1, 27].

$$\begin{aligned}
\frac{dn_p}{df} &= -\frac{2e_2}{f^3} - \frac{3e_3}{f^4} - ... \\
n_g &= n_p + f\left(\frac{dn_p}{df}\right) \\
&= \left(1 + \frac{e_2}{f^2} + \frac{e_3}{f^3} + ...\right) - f\left(\frac{2e_2}{f^3}\right) - f\left(\frac{3e_3}{f^4}\right) - ... \\
&= 1 - \frac{e_2}{f^2} - \frac{2e_3}{f^3} - ...
\end{aligned} \tag{5.20}$$

Then, by dropping higher order terms we obtain these equations.

$$n_p = 1 + \frac{e_2}{f^2} \tag{5.21}$$

$$n_g = 1 - \frac{e_2}{f^2} \tag{5.22}$$

Now for the Earth's ionosphere, the coefficient (e_2) has already been estimated in terms of electron density (n_e) to be roughly equal to -40.3 n_e Hz^2 [1, 27]. However, this value cannot be used since the moon's ionosphere is different. It should be reasonable to state the following. Since the signal being sent from the satellite to the receiver is passing from a vacuum through the lunar ionosphere, down to the surface of the moon, there will be a retardation of the signal velocity per the index of refraction equation. Then, looking at the Earth's value of e_2 in terms of electron density being a negative value for the frequency squared, it is safe to deduce that e_2 for a lunar ionosphere will also be a negative value. Therefore, the term T_f will denote the frequency transformation. This will yield the equation:

$$e_2 = -T_f n_e \ [Hz^2] \tag{5.23}$$

$$=> n_p = 1 - \frac{T_f n_e}{f^2} \tag{5.24}$$

$$=> n_g = 1 + \frac{T_f n_e}{f^2} \tag{5.25}$$

where it is obvious that $1 - \frac{T_f n_e}{f^2} < 1 + \frac{T_f n_e}{f^2}$. Next, swapping these back into velocities gives the following.

$$v_p = \frac{c}{1 - \frac{T_f n_e}{f^2}} \tag{5.26}$$

$$v_g = \frac{c}{1 + \frac{T_f n_e}{f^2}} \tag{5.27}$$

This means that the group velocity is less than the phase velocity. In terms of GPS signals it means that the carrier phase signal will reach the receiver before the PRN code does [1].

One method of correction is by using two different phase frequencies [1]. By differencing these phases, the ionospheric errors can be estimated by the following equation:

$$\Delta ion = \left(\frac{f_2^2}{f_2^2 - f_1^2} \right) (P_{f1} - P_{f2}) \tag{5.28}$$

$$\delta t_{ion} = \frac{\Delta ion}{c} \tag{5.29}$$

where f is the corresponding frequency of each signal, P is the pseudoranges calculated with respect to each frequency, and Δion is the estimated error in terms of meters [1]. It is easily converted into time by divided by the speed of light.

According to Stubbs, the dust in the atmosphere around the moon gets ionized from the sun's ultraviolet rays that hit the dust [20]. This is similar to how the ionosphere is formed on Earth, except here on Earth it is the gas atoms and molecules that become ionized in the atmosphere [1]. Originally, he based his research from the Apollo 15 photographs taken from the lunar surface of the glow over the lunar horizon [20, 21]. From these photographs the presence of dust in the lunar ionosphere was estimated with the assumption that the dust grains were 0.1μm [20, 21]. Moreover, after including data acquired from the Soviet probes Luna 19 and 22, it was determined that the original rough order estimate was lower than expected. Using the data from these probes it was determined that the dust-electron column concentrations (density (n_e)) peaked at roughly 10^3cm^{-3} at an altitude of roughly 5km [20]. In addition, there were ionized dust concentrations detected at an altitude of up to 100km [20]. It was also calculated that these dust concentrations drop exponentially as altitude increases [20]. The research states that this is roughly 20 times more than originally expected [20].

The implications of the lunar ionosphere will have on radio signals means that equation (5.22) may require amending since the ionosphere may not produce continuously the same results, or may just be intrinsically different from the Earth's ionosphere. Furthermore, when humans or even probes return to the moon, large amounts of dust will be thrown into the air. Moreover, if colonization occurs, even more dust will make its way into the air. This may increase the amount of dust that gets ionized, causing the lunar ionosphere to become stronger. In turn, this will cause greater disturbances in all signals sent to the lunar surface including this GPS.

Ultimately, actual data and analysis will be needed to truly quantify this phenomena in order to derive a better estimation of the errors related to it. Already, there are two lunar probes with missions to study the lunar ionosphere. The first is the ARTEMIS probe which is currently in lunar orbit. Among its several goals, one of its missions is to study the dust in the lunar ionosphere. In addition, to ARTEMIS, the Lunar Atmosphere and Dust Environment Explorer (LADEE) probe which is scheduled for a 2013 launch is going to specifically conduct more observations of the lunar ionosphere, and determine the dynamics of it [31]. This will also help to determine the different effects the lunar ionosphere may have on communication and signals as opposed to a typical ionosphere [14].

5.2 Lunar Pseudorange Determination

In general, calculating pseudoranges will be the same as described in chapter two. The specifics in this section which will differ are the addition of the error term, using specific issues pertaining to the proposed system in this thesis (Ie. altitude, CSAC,

etc...).

5.2.1 Position and Time

Recapping from section 2.8.2, the linearized equation for the pseudorange calculation is below.

$$\begin{pmatrix} \Delta P_1 \\ \Delta P_2 \\ \Delta P_3 \\ \vdots \\ \Delta P_m \end{pmatrix} = \begin{pmatrix} \frac{\partial P_1}{\partial x} & \frac{\partial P_1}{\partial y} & \frac{\partial P_1}{\partial z} & \frac{\partial P_1}{\partial t_u} \\ \frac{\partial P_2}{\partial x} & \frac{\partial P_2}{\partial y} & \frac{\partial P_2}{\partial z} & \frac{\partial P_2}{\partial t_u} \\ \frac{\partial P_3}{\partial x} & \frac{\partial P_3}{\partial y} & \frac{\partial P_3}{\partial z} & \frac{\partial P_3}{\partial t_u} \\ \vdots & \vdots & \vdots & \vdots \\ \frac{\partial P_m}{\partial x} & \frac{\partial P_m}{\partial y} & \frac{\partial P_m}{\partial z} & \frac{\partial P_m}{\partial t_u} \end{pmatrix} \begin{pmatrix} \Delta x \\ \Delta y \\ \Delta z \\ \Delta t_u \end{pmatrix} + v$$

This equation can be generalized as:

$$\Delta P = A\Delta x + v \tag{5.30}$$

where ΔP are the pseudorange observables, Δx are the position and time offsets, v is the error values or noise, and A is a matrix describing the relationship between Δx and ΔP. Another perspective that may be taken is ΔP is a vector containing our raw, pseudorange measurements, and A, Δx, and v are the components that constitute the raw measurement. The least squares solution to this is below [3]:

$$\Delta x = (A^T A)^+ A^T \Delta P \tag{5.31}$$

where T simply means the transpose of the matrix. This is the standard form of the least squares solution, and can be solved by algorithmic methods such as singular value decomposition (SVD) or QR factorization (Note: there are other methods such as those tailored for sparse matrices, however, GPS, linearized equations are usually

dense matrices, so the aforementioned methods tend to work better) [8]. Two common QR factorization methods are Householder Triangularization and Gram-Schmidt Orthogonalization. While SVD is very stable, it is not as efficient, and Classical Gram-Schmidt (CGS) is efficient, but Modified Gram-Schmidt version has a higher stability, which is necessary since many of GPS related calculations require a high degree of precision [2, 8]. Householder is also a viable option with high stability and efficiency at the same order of magnitude of MGS [8]. For a comparison of these algorithms refer to appendix A. The general algorithm of the QR factorization to solve least squares is as follows [8].

$$A = QR \tag{5.32}$$

$$Ax = b \tag{5.33}$$

$$QRx = b \tag{5.34}$$

$$Rx = Q^T b \tag{5.35}$$

$$x = R^{-1}[Q^T b] \tag{5.36}$$

Moreover, applying this to PVT estimation the following is produced.

$$\Delta x = R^{-1}[Q^T \Delta P] \tag{5.37}$$

Notice the relation between $(A^T A)^+ A^T$ and $R^{-1}Q^T$. This has to do with the orthogonal projection onto A [8].

Now that we have a solution to least squares pseudorange equation for PVT, the next step is to consider the noise factors. In equation 5.25, one may have noticed the error vector v was not present. It was not forgotten, simply moved as shown below (note: v could have been left in the equation, and solved for using least

squares also) [1]:

$$\begin{aligned}\Delta P &= (P_f - P_0) + dP \\ &= dP + \delta P \end{aligned} \tag{5.38}$$

$$\begin{aligned}\Delta x &= (x_f - x_0) + dx \\ &= dx + \delta x \end{aligned} \tag{5.39}$$

where dP & dx represent the offsets without error, and δP & δx represent their errors respectively. Referring back to equation 5.2, δP would contain the error component $c\delta t_e$, and along with it the aforementioned errors.

One pivotal topic that has been stated multiple times in this thesis is that of singularity of pseudorange vectors. In GPS this is called dilution of precision (DOP) [1, 3]. Consider the diagram below. It illustrates when there is a low geometric DOP. The inner and outer circles depict the error range, and the middle circles represent the pseudoranges. When these pseudoranges are non-singular, the colored area of where the receiver is estimated to be is small (note: the dot represents the intersection of the two pseudoranges if there were no errors).

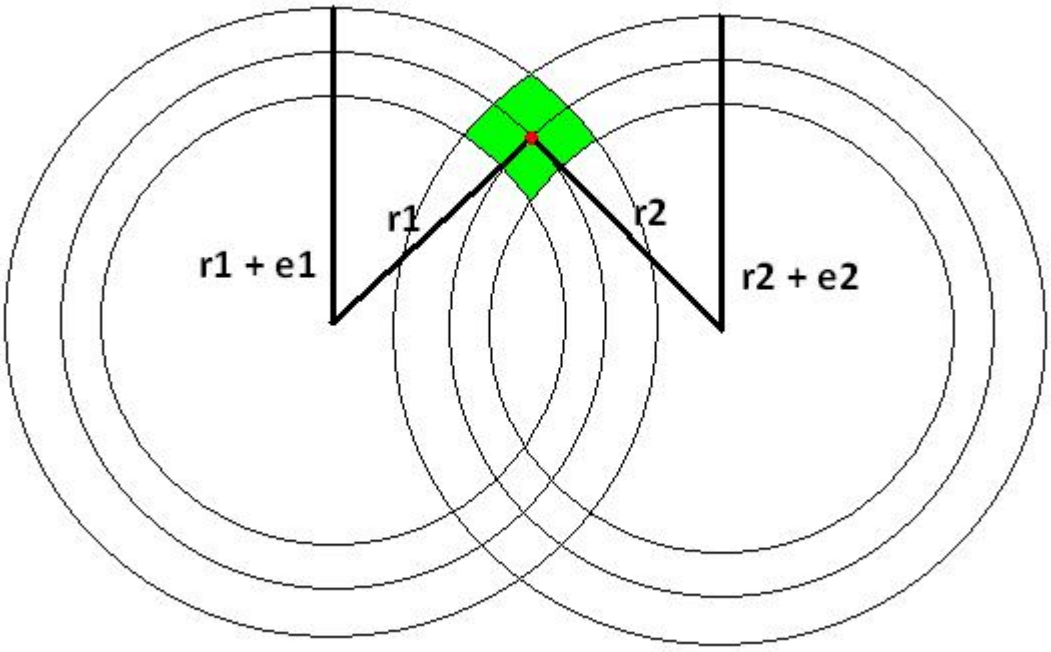

Fig. 5.2: Example of Low Dilution of Precision

The next figure shows an example of when DOP is high. It is trivially, obvious that the colored area is much larger than in the previous figure. This figure conveys the pseudorange vectors beginning to become singular, creating a larger possible area where the receiver could be, and decreasing the accuracy of the system.

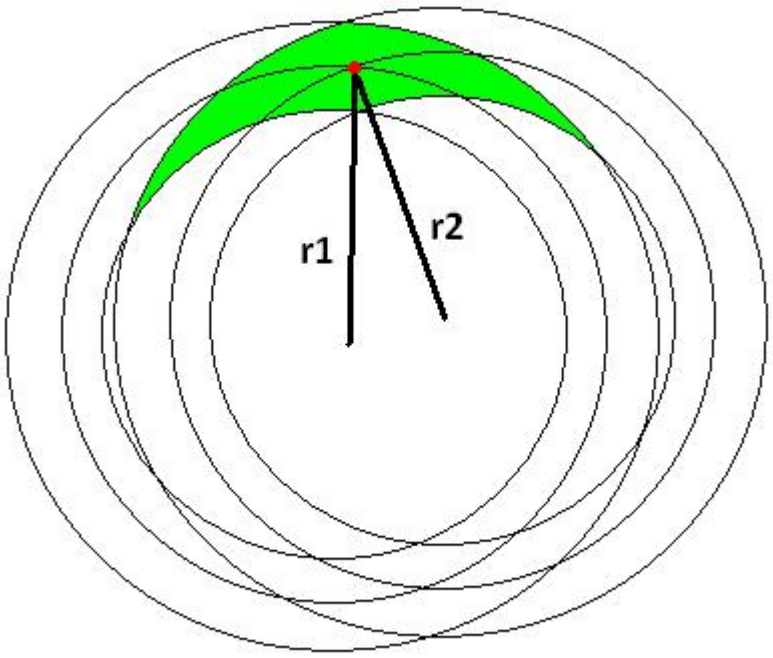

Fig. 5.3: Example of High Dilution of Precision

Now, to delve into DOP with more rigor. In order to fully realize the relation of these errors the covariance must also be considered. The definition of covariance is the expected value of a vector x times its transpose as show below.

$$cov(x) = E[xx^T] \tag{5.40}$$

In our case the covariance for GPS is simply this.

$$cov(\delta x) = E[\delta x \delta x^T] \tag{5.41}$$

In terms of the least squares solution shown earlier the covariance is the following.

$$cov(\delta x) = (A^T A)^+ \sigma^2 \tag{5.42}$$

$$cov(\delta x) = \begin{pmatrix} \sigma_x^2 & \sigma_{x,y}^2 & \sigma_{x,z}^2 & \sigma_{x,ct}^2 \\ \sigma_{y,x}^2 & \sigma_y^2 & \sigma_{y,z}^2 & \sigma_{y,ct}^2 \\ \sigma_{z,x}^2 & \sigma_{y,z}^2 & \sigma_z^2 & \sigma_{z,ct}^2 \\ \vdots & \vdots & \vdots & \vdots \\ \sigma_{ct,x}^2 & \sigma_{ct,y}^2 & \sigma_{ct,z}^2 & \sigma_{ct}^2 \end{pmatrix}$$

Notice how the main diagonal has only one subscript term. Using these terms produces the geometric DOP.

$$GDOP = \frac{\sqrt{\sum_i^m \sigma_{i,i}^2}}{\sigma} \tag{5.43}$$

$$= \frac{\sqrt{\sigma_x^2 + \sigma_y^2 + \sigma_z^2 + \sigma_{ct}^2}}{\sigma} \tag{5.44}$$

The geometric DOP is essentially a measure of geometry relationship between the satellites and the receiver [1, 3]. There are other metrics of DOP which measure various aspects of the noise and singularity of their respective vectors such as altitude, relative position, time, and velocity [1]. Each one of these parameters uses the same general equation (5.29), and by simply plugging in the pertinent variances.

5.2.2 Velocity Estimation

One method for estimating the receiver's velocity is simply by use of its derivation from the kinematic position function [26].

$$x(t) = \frac{at^2}{2} + v_0 t + x_0 \tag{5.45}$$

$$v(t) = \frac{dx}{dt} = at + v_0 \tag{5.46}$$

Then, applying this to our GPS estimation the following derivation is produced:

Proof.

$$
\begin{aligned}
w_d &= \frac{du}{dt} \\
&\approx \frac{u_2 - u_1}{t_2 - t_1} \\
&= \Delta x_i - \Delta x_{i-1} \\
v_u &= \frac{||w_d[1:3]||}{w_d[4]}
\end{aligned}
$$

□

where w_d is the derivation vector, Δx represents the current and previous iteration of the position and time vector, and v_u is the velocity of the user (receiver) calculated from the norm of the position difference divided by the change in time.

6. OPTIMIZATION

6.1 The Kalman Filter

Least squares works by a snapshot of the current pseudorange measurements, and performs an estimation from those. It is obvious that past data can improve the accuracy and precision of most all estimations. The Kalman filter provides a means of using a priori and a posteriori data to determine an optimal estimation [36]. The Kalman filter is essentially a recursive algorithm which performs an initial estimate, then applies a correction factor [37]. This process is repeated recursively until the algorithm converges to the optimal solution [37].

6.1.1 Basics

The basic form of the Kalman filter is below.

$$current = previous \ + \ correction(current \ measurement \ - \ previous) \qquad (6.1)$$

This equation is stating that the current estimate is based upon the previous measurement and the current measurement scaled by a correction factor. Also, from this basic form, the recursion should readily be apparent. The equation starts off by performing a initial estimation or prediction. Next, a correction of the original estimate takes place with a new measurement. This repeats until an optimal solution

is computed. Below is the correction component of the equation.

$$correction = previous\ variance\ /\ (previous\ variance\ +\ current\ variance) \quad (6.2)$$

In this instance the variance is a measure of the amount of error or noise from a particular measurement or estimation. The variance from these measurements produces a correction factor by applying a weighted value to the current measurement and the previous estimation. Notice that current variance is in the denominator of the function. This means that as the current measurement's variance increases, so does its noise. The noisier the measurement is, the less it can be trusted as a legitimate value, therefore, it is not desired for the current measurement to have a large effect on the overall estimation. This also has the opposite effect where if the variance of it is small, then the measurement has less noise, and the current measurement has more of an impact on the estimation providing a better correction.

For these noise variances a couple of assumptions need to be asserted. The first is that there is a Gaussian (normal) distribution of the noise [37]. This accounts for the errors being uniformly distributed and random giving a normally shaped bell curve [37]. The second is that the noise is assumed to be white noise. White noise is the noise that is distributed evenly across all frequencies [37]. Analogically, when all colors of visible light are evenly distributed in intensity, and mixed together, the color produced is white. In a sense, this makes the individual error values 'truly' random. These assumptions will continue to apply for the rest of the discussion regarding the Kalman filter.

Now, with the concept introduced, the actual function will be shown:

$$\hat{x}(t_i) = \hat{x}(t_{i-1}) + K(t_i)(m(t_i) - \hat{x}(t_{i-1})) \tag{6.3}$$

where all terms are a function of time, i is the current epoch, i-1 is the previous epoch, x is the function for the estimation, m is the current measurement function, and K is the correction function which is presented next.

$$K(t_i) = \frac{{\sigma^2}_{\hat{x}}(t_{i-1})}{{\sigma^2}_{\hat{x}}(t_{i-1}) + {\sigma^2}_m} \tag{6.4}$$

As discussed before, K is the correction function of the current time epoch. It is expressed in terms of the variance of the previous estimation ${\sigma^2}_{\hat{x}}(t_{i-1})$, and the variance of the current measurement ${\sigma^2}_m$. Now this works great for static systems, however, in real life applications including GPS the system is dynamic [1]. The general case for estimation is denoted as [1]:

$$x(t_i) = \Phi(t_i, t_{i-1})x(t_{i-1}) + u(t_i) \tag{6.5}$$

where the functions Φ is the transition matrix, and u is the noise vector [1].

The covariance must also be computed. Recalling from the definition mentioned earlier we can derive the covariance for the Kalman filter denoted $P(t_i)$.

$$cov(x) = E[XX^T] \tag{6.6}$$

$$= P(t_i) \tag{6.7}$$

$$=> P(t_i) = E[XX^T] \tag{6.8}$$

$$= E[(x(t_i) - \hat{x}(t_i))(x(t_i) - \hat{x}(t_i)^T)] \tag{6.9}$$

In the subsequent sections, the Kalman filter will be applied to lunar GPS using these definitions.

6.1.2 Applications To The Global Positioning System

For GPS and dynamic systems the algorithm for the Kalman filter is a two step process [1, 27]. The first step is the prediction step, and second is the correction [36, 37, 38]. Afterwards, the algorithm is recursively iterated. Once each iteration of the prediction-correction is performed, the estimated output converges closer to optimal value. The equations for the prediction step are as follows [1, 27, 36, 37, 38].

$$\hat{x}(t_i^-) = \Phi(t_i, t_{i-1})\hat{x}(t_{i-1}^+) \tag{6.10}$$

$$P(t_i^-) = \Phi(t_i, t_{i-1})P(t_{i-1}^+)\Phi^T(t_i, t_{i-1}) + Q(t_{i-1}) \tag{6.11}$$

These are for the correction step [1, 27, 36, 37, 38].

$$\hat{x}(t_i^+) = \hat{x}(t_i^-) + K(t_i)(m(t_i) - S(t_i)\hat{x}(t_i^-)) \tag{6.12}$$

$$K(t_i) = \frac{P(t_i^-)S^T(t_i)}{S(t_i)P(t_i^-)S^T(t_i) + R(t_i)} \tag{6.13}$$

$$P(t_i^+) = (I - K(t_i)S(t_i))P(t_i^-) \tag{6.14}$$

All the terms should be familiar, with the exception of the +/- superscripts. Assuming t_i is the current time at the time of measurement, then t_i^- denotes the time just before the measurement. Conversely, t_i^+ indicates the time just after the measurement. Why go through the trouble of such a scheme? The reason is it allows us to indicate when particular measurements occurred in relation to an estimate that was made. Moreover, particular measuring events can be assigned to different time epochs.

6.1.3 Proposed Design Using Kalman Filtering

Regarding the algorithm utilizing Kalman filtering to determine PVT, there are two major approaches that can be taken. The first is to estimate the PVT values using the filter, correct these estimates, then repeat until the optimal solution is produced [1]. The second is similar to the first except for performing these computations on the actual PVT values, it is applied to the errors [1]. Then once the errors are calculated, these are subtracted from the measured PVT values [1]. Consider the following high-level design diagram [1].

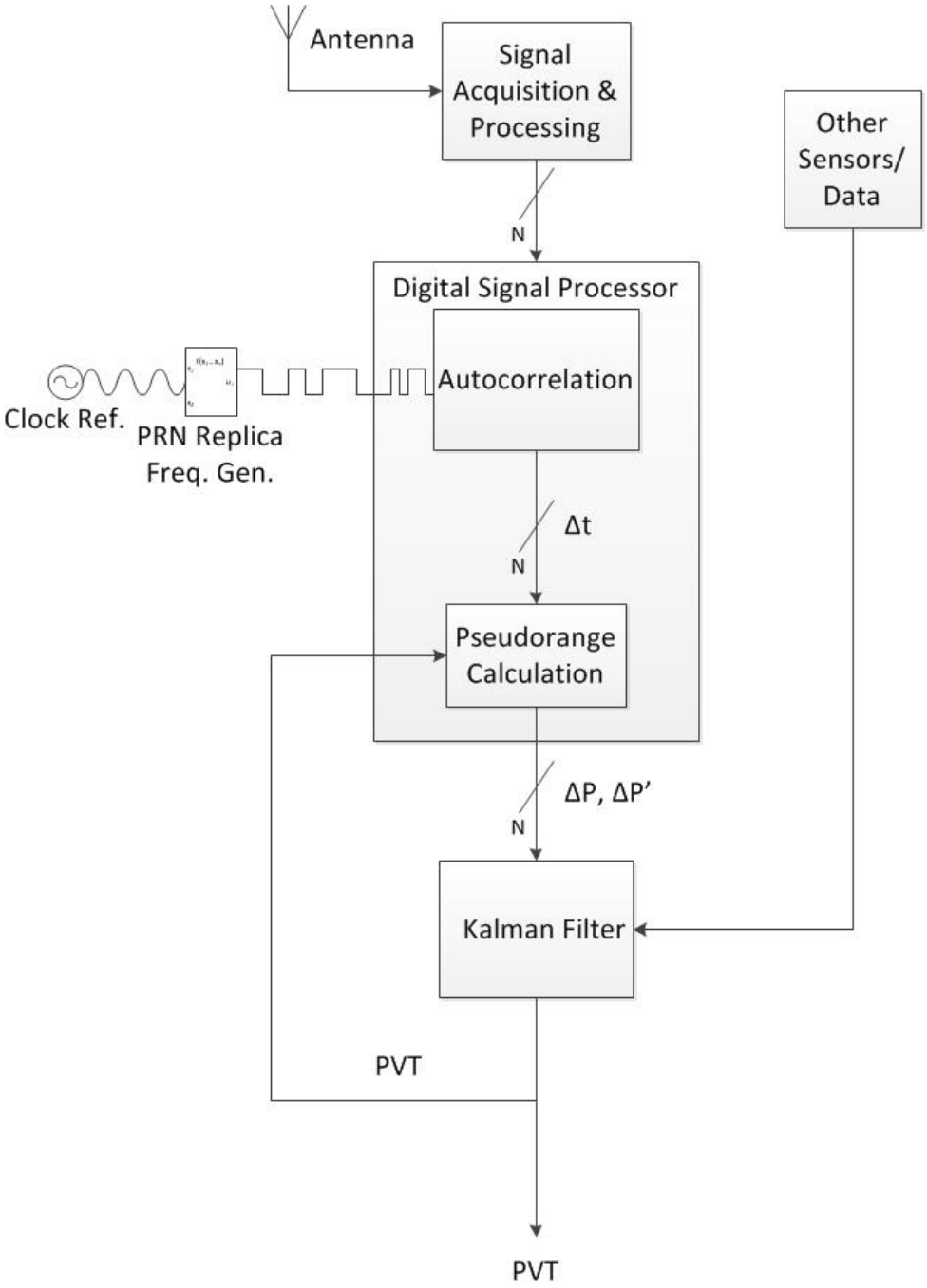

Fig. 6.1: High-Level Design of Kalman Filter and Position, Velocity, and Time Calculation Within Receiver

The first step is the transmitted signal from the satellite reaches the receiver. Second, the signal is acquired and preprocessed. Notice the slash N over the progression arrows. This indicates a data bus of N wide. A bus is used so that multiple satellite's signals can be processed at once. Once this is complete the signal(s) are passed along. Third is the autocorrelation stage. Here, two inputs are injected. The first is the replicated PRN code which is generated from a clock reference such as a crystal oscillator. The second is the aforementioned bus containing the satellite signals and their PRN codes. These codes are passed along the bus to the digital signal processor (DSP).

Upon reaching the DSP, the code is autocorrelated with the replica which determines if the signal is indeed from a known GPS satellite and which one it pertains to. Also, the time differences and time noise values are output to the next stage. The fourth stage is where the pseudorange and its first derivative are calculated from the time values using the numerical equations from chapter two and five (Note: it is also possible for the DSP to compute initial PVT estimates using least squares methods from chapter five). The pseudoranges are then output to the Kalman filter.

The fifth stage performs the Kalman filter algorithm to the pseudoranges. The pseudoranges are inputted into the Kalman filter as the initial estimates. Recall from the previous section the prediction-correction at the heart of the Kalman filter. Then, the correction step is completed producing a better estimate. This 'better' estimate is outputted to whatever other subsystem or displayed for use. Additionally, this estimate is also fed back to the pseudorange calculation stage. The feed-back system allows the previous estimate to be synthesized with the current estimate to produce

another improved estimate. This process recursively continues until an optimal PVT estimate is produced.

Lastly, notice the additional stage labeled "Other Sensors/Data". This stage represents additional data that can be measured, calculated, and input into the Kalman filter. These sensors can be accelerometers, radiation detectors, gyroscopes, compasses, and other instruments, which can detect and measure other types of movement such as rotations, accelerations, or radioactive particles. The data can then be sent into the filter to provide a manifold of information to aid in the correction of PVT estimation. This is referred to as GPS integration [1].

6.1.4 Lunar Differential Global Positioning System

At the end of the former section GPS integration was introduced. Here this topic will be synthesized with differential GPS. Differential GPS in its basic form is another type of integration technique where ground based stations are used to provide additional information to aid in PVT estimation and error correction [1]. One method of implementation is to use signal transmitters that are on the ground called pseudolites [1]. Commercial and military aircraft already use such a system for their navigation purposes [1]. Pseudolites work in conjunction with the satellites to perform the differential GPS trilateration [1, 3]. Also, communications networks can be used to increase accuracy and precision of the GPS. The Earth-based GPS uses this method extensively. A lunar GPS would also benefit from differential GPS to boot.

There is currently research being conducted by Ron Li of Ohio State University on designing a lunar GPS system that would utilize some of these techniques [41].

It is referred to as the Lunar Astronaut Spatial Orientation and Information System (LASOIS) [42]. Their system works by integration of various on-board sensors, where they are placed on the astronaut's suits, lunar rovers, pseudolites, and existing moon orbital satellites [42]. The sensors range from cameras, to star trackers, geographic data, odometers, inertial measurement units, and more [42, 43, 44]. All of these sensors create a network that is capable of sending signals to one another and the Earth-based control station, relaying navigation information [42, 43, 44]. The synthesis of this data is then used for the astronauts navigation on the surface of the moon. This system would also be deemed part of the state Other Sensors/Data, and would send this data to be input into the Kalman filter method previously described. If such a system were to be integrated with the proposed CubeSat-Lunar GPS in this thesis, then its accuracy and precision would be greatly increased.

7. CONCLUSION

The major goal of this thesis was to conduct a feasibility study for designing a CubeSat navigation system for the moon. Subsequently, a comprehensive review of newly emerged research in regards to a lunar GPS was conducted. This thesis considers not only the scientific topics, but also its engineering implications. It was determined through this research that such a system can be developed using the CubeSat platform, and the chip-scale atomic clock. The satellites are proposed to be deployed at an altitude of 3.34×10^4 km using Rider inclined-circular orbits, and Kepler's orbital equations. This produces an orbital period of roughly one-fourth of a moon day. At this altitude, the CubeSat transmitter power was considered by means of a free-space propagation loss analysis referencing the inverse square law. This showed the maximum allowable path loss which would govern commonly, installed, CubeSat transceivers with frequencies between 400 MHz and 1.6 GHz.

Furthermore, analysis of research regarding the CSAC as it pertains to a CubeSat Lunar GPS was accomplished through a comparison with the Galileo GPS RAFS [1]. The rough order of magnitude times for clock updates have been generalized to 5.56 $\frac{min}{m}$. This shows that the CSAC is a viable option for use as an AFS in addition to its small size and low power consumption. Additionally, the lunar ionosphere was examined for its properties related to this subject. The lunar ionosphere will need to

be compensated for, and the LADEE space probe is scheduled to gather data on this phenomena on how it may effect signals and communications. Its effects can be estimated by electron density and a frequency transformation, and initially compensated for by transmitting two different carrier frequencies.

Next, this thesis reviewed error corrections, pseudorange, and PVT calculations as the Lunar GPS would be concerned. The Kalman filter and the LASOIS were presented as options for optimizing PVT determination on the moon through means of a recursive prediction-correction algorithm and differential GPS integration via a sensor network respectively. Finally, various test programs to support this research and study were written in Scilab. The programs include: Rider constellation analysis, maximum free path loss rough order of magnitude, clock drift for the CSAC, L1 Lagrange calculation, the numerical algorithms for QR factorization, and their stability test. These are included in the accompanying CD.

7.1 Review of Contributions

The major contribution of this thesis was to determine the feasibility of lunar navigation system utilizing CubeSats. This thesis can be used as a motivation and reference for a governing system requirements document and a preliminary design. It was shown that the CSAC provides a means of an accurate and precise AFS, while fitting within the CubeSat specified dimensions. The constellation design for this system was shown to provide a minimum level of global coverage for the moon and GPS requirements. Specifically this research was accepted for publication in the WorldComp'12 conference [46]. Furthermore, the VAT was discussed as an option for trajectory

correction of the satellites. The new research regarding the lunar ionosphere and its possible effects was examined. Next, position, velocity, and time measurements using least squares methods was shown. Lastly, optimization techniques specifically, Kalman filtering, and the integrated GPS by Ron Li were discussed.

7.2 Future Directions

Since the results of this research show that a lunar GPS utilizing CubeSats can be done, the next step will be to start preliminary designs for the satellites themselves. The future of this research will include, but not be limited to optimizing the number of satellites in each plane considering areas of zonal coverage, transceiver and antenna design, increasing the time between clock updates, additional effects of the lunar ionosphere, and improving error measurement. Another option for enhancing timing precision could involve the use of inserting a more accurate and space-proven atomic clock and transceiver in the CubeSat launcher. Subsequently, the on-board AFS on the space vehicle taking astronauts could be used too. This would then interface with the other satellites and control segments to provide more accurate timing. Furthermore, a simulation (software and hardware) could be done for design reviews. Integration of the LASOIS GPS with the proposed system in this thesis is another point of interest. Another issue to consider is that of launching and deploying the satellites into their proposed orbital planes. The current trend for rocket launches is pushing towards the private sector, where the cost per pound to launch payloads into space will be substantially cheaper. These companies and their technology should be considered as a new viable option for deploying the CubeSats.

APPENDIX A

QR FACTORIZATION NUMERICAL ALGORITHMS

A.1 Methods

As mentioned earlier, the proposed method for calculating the linear least squares problem for PVT determination is QR factorization. The QR factorization has the following form:

$$A = QR \tag{A-1}$$

where A is the matrix being solved for, Q is the mxm matrix containing orthonormal vectors to A, and R is an upper triangular mxn matrix [8]. The following is the Classical Gram-Schmidt (CGS) iteration for calculating the column vectors of Q (denoted q) and the elements of R (denoted r) [8]:

$$q_j = \frac{a_j - \sum_{i=1}^{j-1} r_{ij} q_i}{r_{jj}} \tag{A-2}$$

$$r_{ij} = q_i^T a_j \tag{A-3}$$

$$|r_{jj}| = ||a_j - \sum_{i=1}^{j-1} r_{ij} q_i|| \tag{A-4}$$

where i, and j are simply indices of the row and column. As it will be shown in the next section, CGS is mathematically sound, but numerically unstable [2, 8]. Fear not, there is a modified Gram-Schmidt (MGS) for performing a QR factorization which is numerically stable. Below are the equations [8]:

$$v_j = P_{\perp q_{j-1}} \dots P_{\perp q_2} P_{\perp q_1} a_j \tag{A-5}$$

$$= v_j^- - q_{j-1} q_{j-1}^T v_j^- \tag{A-6}$$

where v is the orthogonal projection (denoted P) from the vector a. Then q and r are calculated by the following.

$$r_{ii} = ||v_i|| \tag{A-7}$$

$$r_{ij} = q_i^T v_j \tag{A-8}$$

$$q_i = \frac{v_i}{r_{ii}} \tag{A-9}$$

The last method considered is the Householder triangularization which performs a full QR factorization. The Gram-Schmidt orthogonalization performs the successive computations on the R matrix, whereas householder generates an upper triangular Q matrix. Here is the Householder reflector [8, 47]:

$$H = I - 2vv^T \tag{A-10}$$

$$v_i = e_1||x||(\pm x_1) + x \tag{A-11}$$

$$v_i = \frac{v_i}{||v_i||} \tag{A-12}$$

where H is the reflection matrix, x and v are the original and reflected vectors orthogonal to the hyperplane respectively.

A.1.1 Stability Test

One method for testing the stability between QR factorization algorithms is by testing their orthogonalization of the R matrix main diagonal entries with singular values [8]. As each r_{jj} element and the corresponding q_j column vector are calculated, there are rounding errors that innately occur [8]. A Scilab program constructed here initializes a 100x100 matrix filled with normally distributed random numbers to perform this test. The r_{jj} values are graphed on a logarithmic scale for classical

and modified Gram-Schmidt, whereas the absolute value of householder's are graphed since it produces negative values. It can be seen that for each higher r_{jj} element is calculated, a higher level of precision is calculated from the respective algorithm. This is attributed to the estimated result not being as precise from the incurring rounding errors. The key concept here is that the algorithm should maintain a sufficiently high level of precision as more iterations are computed. Consider the diagram below.

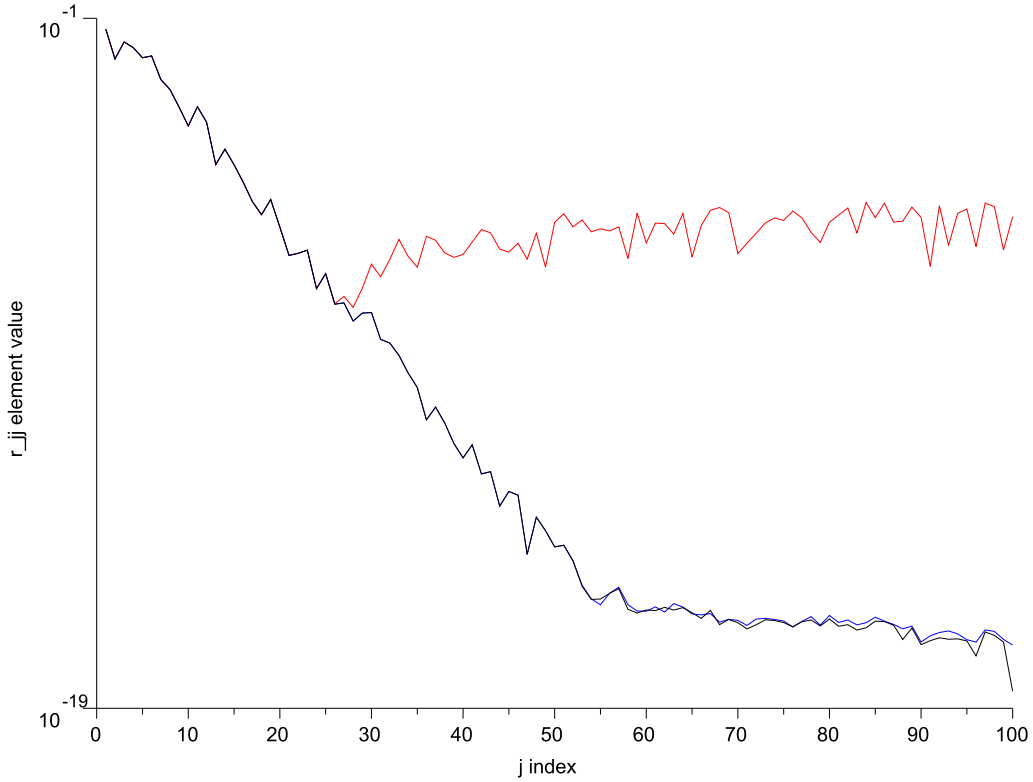

Fig. A.1: r_{jj} Elements versus j Indices for Classical, Modified Gram-Schmidt, and Householder Algorithms Stability Tests of 100x100 Matrix

In the above figure, the red line is for CGS, the blue line is for MGS, and the

black line is for householder. As it can be seen, the stability and precision of CGS breaks down around the order of 10^{-8}. As for MGS and householder, the epsilon value (machine precision roughly 10^{-16}) is easily reached. Householder shows that it can produce a slightly higher level of precision than MGS. Now as applied to GPS calculations, a 100x100 sized matrix would not occur since the most columns that would exist would be four (x, y, z, t) coordinates. Also, there would almost certainly never be 100 rows corresponding to 100 satellites. So, this test was ran again, but instead with a 30x4 matrix, the results are shown below.

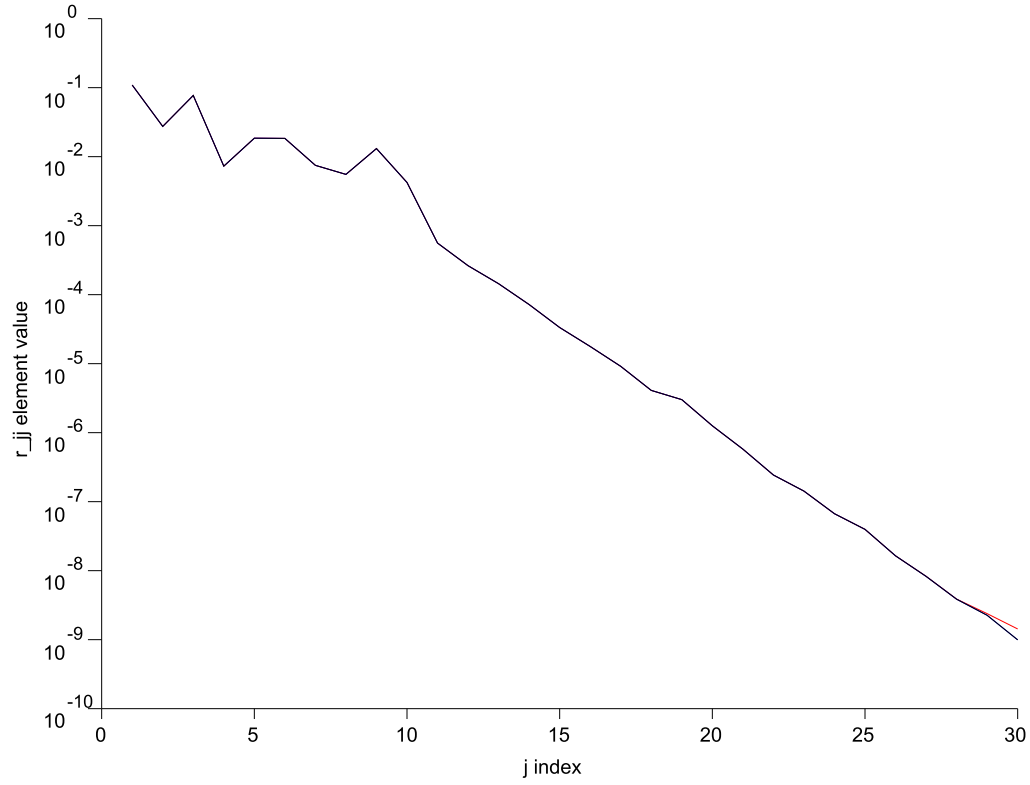

Fig. A.2: r_{jj} Elements versus j Indices for Classical, Modified Gram-Schmidt, and Householder Algorithms Stability Tests of 30x4 Matrix

These results show that all three algorithms remain close to each other until almost 30 where they begin to separate. This may indicate that CGS could be used, but it may still be better to choose MGS or householder since the order of magnitude at the precision separation for CGS is around 10^{-8} and 10^{-9} which can produce errors of roughly tens of meters. Moreover, multiple iterations would be occurring which would cause the errors to compound. Finally, the code for the three algorithms and the stability test can be found on the attached CD.

APPENDIX B

KALMAN FILTER NUMERICS

B.2 Kalman Filter Numerical Algorithm For Global Positioning Systems

In chapter six the idea of the Kalman filter was introduced as a GPS optimization technique for determining PVT. Here, the numerical process for calculating the Kalman filter will be presented. As formerly stated, there are two primary methods for PVT estimation with the filter: predict actual PVT values, or their errors, then correct for these recursively. If the latter technique is used, then simply subtract the optimal error estimates from the PVT values before displaying the results. In either case, the algorithm will not adversely differ. As it pertains to Lunar GPS, adding in the error corrections from chapter five may also be incorporated for increased precision.

B.2.1 Prediction Step

To begin with, consider the initial estimate equation:

$$\hat{x}(t_i^-) = \Phi(t_i, t_{i-1})\hat{x}(t_{i-1}^+) \tag{B-13}$$

$$\Delta x_i = A\Delta x_{i-1} \tag{B-14}$$

From here, what needs to be done is to form the state vector $\hat{x}$ and the transition matrix Φ as shown below [1]. Since this is similar to $x = A^{-1}b$, then substituting with the pseudorange linear equation gives:

$$\Delta x_i = A^{-1}\Delta P \tag{B-15}$$

where $A^{-1} = \Phi$ and $\Delta P = \Delta x_{i-1}$. This would be solved using the numerical techniques previously described. The assumption of $A^{-1} = \Phi$ is acceptable since the extended Kalman filter state transition matrix can be computed by the Jacobian of

the state vector [36]. Furthermore, this substitution gives our initial position estimates. The next step is to calculate the covariance matrix.

$$P(t_i^-) = \Phi(t_i, t_{i-1})P(t_{i-1}^+)\Phi^T(t_i, t_{i-1}) + Q(t_{i-1}) \tag{B-16}$$

$$P_i = AP_{i-1}A^T + Q_{i-1} \tag{B-17}$$

Then, form the initial error covariance matrix P_{i-1} as follows:

$$P_{i-1} = \sigma_{\delta x}^2 I \tag{B-18}$$

where $\sigma_{\delta x}^2$ is the variance of the error vector which can be calculated from the errors mentioned in chapter five. Lastly, the noise covariance matrix is formed:

$$Q_{i-1} = cov(v)I \tag{B-19}$$

where $v << 1$ and is a random variable of white noise (normally distributed noise). It is also acceptable to use pre-tabulated noise data based upon the hardware specifications [1]. This allows the covariance matrix to be calculated completing the prediction step.

B.2.2 Correction Step

Once the prediction step is complete, its results can be inputted to produce a more accurate estimate. First, consider the Kalman gain equation:

$$K(t_i) = \frac{P(t_i^-)S^T(t_i)}{S(t_i)P(t_i^-)S^T(t_i) + R(t_i)} \tag{B-20}$$

$$K_i = \frac{P_i S_i^T}{S_i P_i S_i^T + R_i} \tag{B-21}$$

The current measurement noise covariance matrix R_i, is formed from the pseudorange variances (denoted P and P').

$$R_i = \begin{pmatrix} \sigma_P^2 & 0 \\ 0 & \sigma_P'^2 \end{pmatrix}$$

The next step is to form the measurement matrix S_i. This is similar to the state transition matrix, however, a current time epoch is needed, therefore, we can simply request an updated pseudorange calculation from the digital signal processor:

$$a_i^+ = \begin{pmatrix} \frac{\partial P}{\partial x} & \frac{\partial P}{\partial y} & \frac{\partial P}{\partial z} & \frac{\partial P}{\partial t_u} \end{pmatrix}$$

where a_i^+ is the row vector from A, and is from a new measurement.Subsequently, we form S_i as an nxm matrix in the following pattern [1].

$$S_i = \begin{pmatrix} \frac{\partial P}{\partial x} & 0 & \frac{\partial P}{\partial z} & 0 \\ 0 & \frac{\partial P}{\partial y} & 0 & \frac{\partial P}{\partial t_u} \end{pmatrix}$$

Now that the unknown matrices are formed, the K_i may be calculated. Then, we calculate the new epoch covariance matrix:

$$P(t_i^+) = (I - K(t_i)S(t_i))P(t_i^-) \tag{B-22}$$

$$P_{i+1} = (I - K_i S_i)P_i \tag{B-23}$$

Before the next estimate is calculated, the observation vector m_i needs to be calculated. This may be done similar to how x_i was calculated.

$$m_i = S_i \Delta x_i \tag{B-24}$$

In this equation it should be noticed that m_i is merely a new pseudorange estimate.

Then, a corrected estimate may be calculated as follows:

$$\hat{x}(t_i^+) = \hat{x}(t_i^-) + K(t_i)(m(t_i) - S(t_i)\hat{x}(t_i^-)) \tag{B-25}$$

$$\hat{x}_{i+1} = \hat{x}_i + K_i m_i - S_i \hat{x}_i \tag{B-26}$$

This completes the correction step, and the estimated value may be displayed to the user or sent to any pertinent subsystem. It should be noted, other implementation possibilities due exist. This essentially covers one iteration of the algorithm. Furthermore, it may be recursively fed-back into the Kalman filter prediction step along with new measurements and data to converge to an even more accurate estimate [36]. The more accurate the initial estimate, the less iterations are needed to converge to an optimal solution. Albeit, a less accurate initial estimate can still be used to produce good results which encompasses the beauty of the Kalman filter.

REFERENCES

[1] E. D. Kaplan and C. Hegarty. *Understanding GPS: Principles and Applications, Second Edition*. Artech House Publishers. 2005.

[2] K. E. Schubert. CSE635 Numerical Algorithms and Simulation. CSUSB. April 2011.

[3] G. Blewitt. "Basics of GPS Technique: Observation Equations". Dept. of Geomatics, University of Newcastle, United Kingdom. 1997.

[4] P. A. Kline. "Linearizing The GPS Pseudorange Equations". Virginia Polytechnic Institute and State University. Feb. 1997.

[5] NASA. Earth: Facts and Figures. Sept. 2011. <http://solarsystem.nasa.gov/planets/profile.cfm?Object=Earth&Display=Facts&System=Metric>.

[6] C. Langton. "Unlocking the Phase Lock Loop - Part 1". 1998, 2002. <http://www.complextoreal>.

[7] The Radio Amateur Satellite Corporation (AMSAT). CubeSat Information. 2004, Dec. 2010. <http://www.amsat.org/amsat-new/satellites/CubeSats.php>.

[8] L. N. Trefethen and D. Bau III. *Numerical Linear Algebra*. 1997.

[9] A. V. Balakrishnan. *Kalman Filtering Theory*. Optimization Software. 1987.

[10] K. S. Miller and D. M. Leskiw. *An Introduction To Kalman Filtering With Applications*. Krieger Publishing Company. 1987.

[11] Wikimedia Commons. Elipse.svg. Pubilc Domain. Aug. 2009. <http://commons.wikimedia.org/wiki/File:Elipse.svg>.

[12] Wikimedia Commons. Bebenko. Orbits-OrbitalDistances-001.sk.PNG. Creative Commons and GNU Free Documentation License. Ver. 1.2. Apr. 2005, Apr. 2012.

[13] Merriam-Webster. "navigation". 2012. <http://www.merriam-webster.com/dictionary/navigation>.

[14] NASA. Mystery of the Lunar Ionosphere. Nov. 2011. <http://science.nasa.gov/science-news/science-at-nasa/2011/14nov_lunarionosphere/>.

[15] L. Rider. "Analytical Design of Satellite Constellations for Zonal Earth Coverage Using Inclined Orbits". The Journal of the Astronautical Sciences. Volume 34. Mar. 1986.

[16] California Polytechnic State University San Luis Obispo, Stanford University. CubeSat. Dec. 2010.<http://www.CubeSat.org/index.php>.

[17] J. Puig-Suari, C. Turner, and W. Ahlgren. "Development of the Standard CubeSat Deployer and a CubeSat Class PicoSatellite". California Polytechnic State University San Luis Obispo. 2001.

[18] S. Knappe, P. D. D. Schwindt, V. Shah, L. Hollberg, and J. Kitching. "A chip-scale atomic clock based on ^{87}Rb with improved frequency stability". Optics Express Vol. 13, No. 4. Feb. 2005.

[19] J. F. DeNatale, R. L. Borwick, et. al. "Compact, Low-Power Chip-Scale Atomic Clock". IEEE 2008.

[20] T. J. Stubbs, D. A.Glenar, W. M.Farrell, R. R.Vondrak, M. R.Collier, J. S. Halekas, and G.T. Delory. "On the role of dust in the lunar ionosphere". NASA. June 2011.

[21] D. A.Glenar, T. J.Stubbs, J. E.McCoy, and R. R.Vondrak. "A reanalysis of the Apollo light scattering observations, and implications for lunar exospheric dust". NASA. Dec. 2011.

[22] J. Sinclair. *How Radio Signals Work*. McGraw-Hill. 1997.

[23] A. Konopliv. Bizarre Lunar Orbits. NASA. <http://science.nasa.gov/science-news/science-at-nasa/2006/06nov_loworbit/>. April 2011.

[24] California Polytechnic State University San Luis Obispo. CubeSat Design Specification (CDS). Rev. 12 Aug. 2009.

[25] F. Rysanek, J. W. Hartmann, J. Schein, and R. Binder. "MicroVacuum Arc Thruster Design for a CubeSat Class Satellite". 16th Annual/USU Conference on Small Satellites. 2002.

[26] H. D. Young, R. A. Freedman. *Sears and Zemanskys University Physics*. 12th Edition. Pearson Addison-Wesley. 2008.

[27] G. Xu. *GPS Theory, Algorithms and Applications*. Second Edition. Springer. 2007.

[28] K. Krane. *Modern Physics. Second Edition*. John Wiley and Sons Inc. 1996.

[29] A. Einstein. *Relativity The Special and the General Theory*. Penguin Books. 1916, 2006.

[30] V. Angelopoulos. The ARTEMIS Mission. NASA. IGPP/ESS UCLA, 2011, 2012.

[31] NASA. Lunar Atmosphere and Dust Environment Explorer (LADEE) Mission. Apr. 2012. <http://nssdc.gsfc.nasa.gov/nmc/spacecraftDisplay.do?id=LADEE>.

[32] J. Vanier. "Atomic clocks based on coherent population trapping: a review". SpringerLink. Applied Physics B: Lasers and Optics. 2005.

[33] Pumpkin Inc. The CubeSat Kit website. 2011. <http://www.cubesatkit.com/index.html>.

[34] Engineering - Attitude and Orbital Control Systems (AOCS). Science Programme European Space Agency (ESA). 2000-2012. <http://sci.esa.int/science-e/www/object/index.cfm?fobjectid=31314&fbodylongid=802>.

[35] D. W. Allan, N. Ashby, and C. C. Hodge. "The Science of Timekeeping". Hewlett Packard Application Note 1289. 1997.

[36] G. Welch, and G. Bishop. "An Introduction to the Kalman Filter". Dept. of Computer Sci, University of North Carolina at Chapel Hill. July 2006.

[37] P. S. Maybeck. *Stochastic Models, Estimation, and Control*. Volume I. Academic Press Inc. 1979.

[38] K. E. Schubert. "Keith On Robotics and Control". CSUSB. R2 Labs. 2012.

[39] W. J. Riley. "Rubidium Atomic Frequency Standards For GPS Block IIR". EG&G Frequency Products. 1990.

[40] Wikimedia Commons. Adrignola. Geo09b4 700.jpg. National Oceanic and Atmospheric Administration. Public Domain. May 2010. <http://commons.wikimedia.org/wiki/File:Geo09b4_700.jpg>.

[41] R. Li, P. F. Gorder. "New Project to Develop GPS-Like System For Moon". Research News, Ohio State University. July 2008. http://researchnews.osu.edu/archive/lunarnav.htm.

[42] R. Li, et. al. "Enhancement of Spatial Orientation Capability of Astronauts on the Lunar Surface Supported by Integrated Sensor Network and Information Technology". NLSI Lunar Science Conference. 2008.

[43] R. Li, et. al. "Lasois: Enhancing the Spatial Orientation Capabilities of Astronauts on the Lunar Surface". 40th Lunar and Planetary Science Conference. 2009.

[44] R. Li, et. al. "The Latest Progress of Lasois: A Lunar Astronaut Spatial Orientation and Information System". 42nd Lunar and Planetary Science Conference. 2011.

[45] V. Daita. “Behavioral VHDL Implementation of Coherent Digital GPS Signal Receiver”. Thesis - University of South Florida. Nov. 2004.

[46] A. Batista, E. Gomez, H. Qiao, K. E. Schubert. “Constellation Design of a Lunar Global Positioning System Using CubeSats and Chip-Scale Atomic Clocks”. CSUSB. WorldComp’12. Apr. 2012.

[47] K. E. Schubert. “Keith On Numerical Analysis”. CSUSB. R2Labs. 2012.

[48] UCSD. “Two-Body Orbital Mechanics”. Lecture 6. 2011. <http://maecourses.ucsd.edu/mae155a/MAE155A_Lecture6.pdf>.

[49] NASA. Moon: Facts and Figures. Apr. 2012. <http://solarsystem.nasa.gov/planets/profile.cfm?Object=Moon&Display=Facts>.

[50] Matthias Borchardt. “The Lagrange points in the Earth-Moon system”. Tannenbusch Secondary School, Bonn. ESA. 2000-2012.

[51] C.F. de Melo, E.E.N. Macau, O.C. Winter, E. Vieira Neto. “Alternative paths for insertion of probes into high inclination lunar orbits”. ScienceDirect. Mar. 2007.